Light-Fueled Liquid Crystal Networks for Aquatic Soft Robotics

by

Natalie Prislinger Pinchin

A thesis

presented to the University of Waterloo

in fulfillment of the

thesis requirement for the degree of

Master of Applied Science

in

Chemical Engineering

Waterloo, Ontario, Canada, 2023

© Natalie Prislinger Pinchin 2023

Author’s Declaration

This thesis consists of material all of which I authored or co-authored: see Statement of Contributions included in the thesis. This is a true copy of the thesis, including any required final revisions, as accepted by my examiners.

I understand that my thesis may be made electronically available to the public.

Statement of Contributions

This thesis is directly related to some of my work that I published during my master's studies.

Chapter 1 and 2 of this thesis are partially reproduced from:

- Pinchin N.P., Guo H., Meteling H., Deng Z., Priimagi A., Shahsavan H., (2023), Liquid Crystal Networks Meet Water: It's Complicated!, Advanced Materials, In-press (10.1002/adma.202303740)

Chapter 3 of this thesis is partially reproduced from:

- Pinchin N. P., Lin C. H., Kinane C. A., Yamada N., Pena-Francesch A., and Shahsavan H., (2022), Plasticized liquid crystal networks and chemical motors for the active control of power transmission in mechanical devices, Soft Matter, 18 (42), 8055-8204 (DOI: 10.1039/D2SM00826B)

I made major contribution in designing and performing experiments, collecting and analyzing experimental data, and writing the papers.

Abstract

The field of soft robotics has developed in response to the need for mechanisms that can operate safely in interaction with humans. Within the field of soft robotics, there is a growing demand for the development of small-scale soft devices capable of non-invasive medical interventions in a variety of technologies, including medical microrobotics, biosensing, and biomedical engineering. Among the many materials used for small-scale soft robotics, liquid crystal networks (LCNs) are of particular interest. LCNs are molecularly anisotropic and demonstrate reversible, programmable shape change upon exposure to external stimuli such as light or heat. However, the actuation of LCNs is often triggered by light, either photochemically or photothermally, which is typically less efficient when operating in flooded environments. Actuation in confined and flooded environments is an important challenge that must be overcome for the implementation of LCNs in real-world biomedical applications. Decoupling the mechanisms of powering, locomotion, and control from robotic functions is a strong solution for achieving efficient operation in flooded media. This work showcases two examples of decoupling locomotion and robotic function for the efficient use of small-scale devices at the air-water interface. This is done through the use of LCNs for control in conjunction with protein motors for powering. An LCN that responds to visible light, rather than UV, is also fabricated and characterized, and will be used for underwater robotic applications in future studies.

In the first case study, protein motors and LCNs are used to power and control a multi-component mechanical device. A milli-scale gear train with integrated motor and clutch functionalities is fabricated and operated at the air-water interface. The driving gear has a protein motor coating and generates propulsive force using the Marangoni effect. This force is transmitted through the gear train unless the clutch gear is activated. The clutch gear is fabricated from a photothermally responsive LCN that has been plasticized through the addition of a nematogenic solvent to improve actuation efficiency. The teeth of the clutch gear bend downwards to disengage from the gear train upon exposure to light, halting the chain of motion on demand. The second case study utilizes photochemical LCNs with applied protein motor coating to construct a V-shaped swimmer that moves across the surface of the water. Photochemical LCNs are used for their meta-stable state that allows for deformations to be held without constant exposure to stimuli. The protein motors are integrated directly onto the LCN swimmer for a single device with orthogonal mechanisms for powering and control. The protein motors generate force that propels the swimmer forward while deformation of the LCN is used for directional control.

In both case studies, UV light is required for shape-change. Looking forward to biomedical applications, a photochemical LCN that is responsive to visible light is also developed and characterized in both air and water. The design of LCN-based small-scale devices with a focus on safe and efficient operation in wet environments will open up new and exciting applications.

Acknowledgements

I would like to thank my supervisor Prof. Hamed Shahsavan for his support and guidance in my research. His supervision and mentorship have been invaluable to me over the past two years. I feel fortunate that I had the opportunity to learn from him.

I am grateful to Professors Ahmad Ghavami, John Saad, and Eric Croiset for the guidance and resources they provided. I am also grateful to the Quantum-Nano Fabrication and Characterization facility team for the generous access to their equipment.

Additionally, I would like to thank the groups I collaborated with: Prof. Abdon Pena-Francesch's group at the University of Michigan and Prof. Arri Priimägi's group at Tampere University. I would also like to thank Prof. Arri Priimägi and the Smart Photonic Materials research group for welcoming me at Tampere for three months. And a heartfelt thank you to my colleagues in the SMART-Lab and at UW in general for all of their help and support. Thank you to Negin in particular for all her help in and out of the lab and the many chats we had over coffee.

Finally, a thank you to my family and friends for their unwavering belief in me, and the hours they spent listening to me talk about my research.

Dedication

Dedicated to my family, for their endless love and support. Especially my grandmother, Ljiljana Prislinger, you would have loved to read this.

Table of Contents

Author's Declaration ii

Abstract iii

Acknowledgements v

Dedication vi

List of Figures x

Chapter 1 Introduction 1

Chapter 2 Literature Review 4

2.1 Aquatic Soft Robotics 4

2.2 Materials for Aquatic Soft Robotics 5

2.2.1 Hydrogels 5

2.2.2 Liquid crystalline materials 6

2.3 LCNs and Water 9

2.3.1 LCN Actuators in Contact with Water 9

2.3.2 Thermal Actuation in Water 12

2.3.3 Photothermal Actuation in Water 12

2.3.4 Photochemical Actuation in Water 16

2.3.5 Research Objective 20

Chapter 3 Plasticized Liquid Crystal Networks and Chemical Motors 22

3.1 Introduction 22

3.2 Materials & Methods 23

3.2.1 Materials 23

3.2.2 Gear Train Fabrication 23

3.2.3 Fabrication and Characterization of LC-Based Gears 24

3.2.4 Materials Characterization 24
3.2.5 Actuation Characterization 24
3.3 Results & Discussion 25
3.3.1 Protein Motors for Power Generation 25
3.3.2 Liquid Crystal Network Clutch Fabrication 27
3.3.3 Liquid Crystal Network Clutch Characterization 29
3.3.4 Orthogonal Actuation of a Hybrid Gear Train Mechanical Device 31
3.4 Conclusion 33
Chapter 4 Photochemical Liquid Crystal Networks and Chemical Motors 34
4.1 Introduction 34
4.2 Materials & Methods 35
4.2.1 Materials 35
4.2.2 Fabrication of LCN-Based Swimmer 35
4.2.3 Materials Characterization 35
4.2.4 Actuation Characterization 36
4.2.5 Swimmer Characterization 36
4.3 Results & Discussion 36
4.3.1 Protein Motors for Movement Generation and Swimmer Design 36
4.3.2 Liquid Crystal Network Design 40
4.3.3 Liquid Crystal Network Characterization 41
4.3.4 Liquid Crystal Network Swimmer Characterization 46
4.4 Conclusion 48
Chapter 5 LCN Soft Actuators Fueled by Visible Light 49
5.1 Introduction 49

5.2 Materials & Methods 49
5.2.1 Materials 49
5.2.2 LCN Actuator Fabrication 50
5.2.3 Materials Characterization 50
5.2.4 Actuation Characterization 50
5.3 Results & Discussion 51
5.3.1 Novel Azobenzene 51
5.3.2 LCN Actuator Fabrication 52
5.3.3 LCN Actuator Characterization 57
5.4 Conclusion 60
Chapter 6 Summary and Outlook 61
References 63
Appendix A Iron Platinum Nanoparticles 74

List of Figures

Figure 2-1 Shape Change Mechanism of Hydrogels 6
Figure 2-2 Shape Change Mechanism of Liquid Crystal Networks 8
Figure 2-3 LCN Actuation Mechanisms 11
Figure 2-4 Movement of Aquatic Photothermal LCNs 16
Figure 2-5 Movement of Aquatic Photochemical LCNs 19
Figure 3-1 Concept of Geart Train with Active Gears 23
Figure 3-2 Protein Motor Coated Gears 26
Figure 3-3 Rotational Speed of Driving Gears 27
Figure 3-4 LCN Clutch Gear Composition 28
Figure 3-5 LCN Clutch Gear Fabrication 29
Figure 3-6 LCN versus PLCN Characterization 31
Figure 3-7 Gear Train with Active Gears 32
Figure 4-1 LCN Swimmer Concept and Bioinspiration 34
Figure 4-2 Protein Motor Coated Particle 37
Figure 4-3 Protein Motor-Driven Particle Movement 37
Figure 4-4 Inactive V-Shaped Swimmer with Protein Motor Coating 39
Figure 4-5 Active LCN Swimmer Fabrication 41
Figure 4-6 Effect of LCN Composition on Bending Behaviour 44
Figure 4-7 LCN Actuation in Air versus Water 45
Figure 4-8 Effect of LCN Aspect Ratio on Bending Behaviour 46
Figure 4-9 LCN Swimmer with Protein Motor Coating 47
Figure 5-1 Novel Azobenzene Structure and Absorption Spectrum 52
Figure 5-2 LCN Fabrication 54
Figure 5-3 LCN Composition and Alignment 56
Figure 5-4 Effect of Wavelength on Bending Behaviour 58
Figure 5-5 Bending Behaviour in Air versus Water 59
Figure 5-6 LCN Lifetime 60
Figure A-1 Nanoparticle TEM Images 74

Chapter 1
Introduction

Robotics has played a major role in shifting technological paradigms over the last several decades. The common premise in the design and manufacturing of all robots has been essentially emulating human or animal forms, bodies, and functions, and elevating them beyond natural capacities. With the advent of robots as auxiliary machines, a variety of industrial tasks requiring high force, speed, and spatiotemporal precision became attainable, at a level which would have been inefficient or even impossible otherwise. Hard robots, traditionally, are mechanical machines made of multiple rigid sensing, actuating, and computational components that, together, perform various tasks. Decades of progress have yielded hard robots capable of remarkably complex motions, control, and functions. However, the noncompliant nature of their building blocks limits their dexterity in situations where safe interaction with humans and soft or fragile objects is indispensable. Hard robots also have difficulty adapting to different shapes and performing tasks in natural environments that at times are cluttered, confined, uneven, or filled with fluids. Designing smaller robots or those with a larger number of miniaturized components and joints may offer some solutions, but ultimately makes hard robots thermodynamically inefficient and costly. Soft robotics is an emerging field in which the challenges hard robots face can be remedied.[1–3]

In soft robotics, the mimicry of human and animal bodies, forms, and functions evolves into the assimilation of soft tissues and organisms, such as muscles and cells.[4,5] Similar to biological creatures, soft robots are either partially or entirely made of compliant materials, as actuators, that facilitate higher degrees of freedom, adaptability, and safer interaction with humans.[6,7] Countless recipes for the design of soft materials, from molecular to macroscopic levels, have provided a vast repertoire of actuators made from either inherently passive or active materials.[8] Thanks to such diversity in design, not only do soft robots enhance the function and performance of their hard cousins, but they also introduce completely unprecedented capabilities.[9] For instance, soft robots made from biocompatible materials can be utilized in various healthcare technologies ranging from sensing to remote communication and control.[10,11] Small-scale soft robots in particular promise minimally invasive medical procedures in confined, complex, and flooded media similar to the human body.[12,13]

A wide range of materials have been developed for use in soft robotics applications; of particular interest are liquid crystal networks (LCNs). LCNs are molecularly anisotropic and demonstrate reversible, programmable shape-change upon exposure to external stimuli such as light or heat. This

shape change is achieved through the molecular patterning of the liquid crystal mesogens. The liquid crystal mesogens undergo an order-to-disorder transition upon exposure to stimuli, such as heat, which is translated into macroscopic shape change based on molecular patterning. There are two main classifications of photo-responsive LCNs, photothermal and photochemical. Photothermal LCNs are doped with a photothermal agent, such as a photothermal dye or carbon nanotubes, that converts the light energy into heat, resulting in shape change. Relaxation then occurs through the dissipation of heat to the LCNs surroundings. Photothermal LCNs have high spatiotemporal control in actuation and typically demonstrate faster actuation than photochemical LCNs. However, they require constant stimuli to maintain deformation and will relax immediately upon ceasing illumination. Photochemical LCNs typically utilize azobenzene photoswitches, which undergo isomerization from the *trans* to *cis*-state to induce shape change. Relaxation then occurs through exposure to light within the *cis*-isomers absorption region or heat for thermal relaxation. While photochemical LCNs, unlike photothermal, are able to maintain deformation when the external stimuli are removed, they typically have slower actuation and rely on the use of UV light, which limits their potential for biomedical applications.

The use of soft robotics in the biomedical field requires them to be able to operate efficiently in flooded media. As such, it is of great importance that the relationship between LCNs and water be well understood. While this relationship is still being studied, it is known that water typically reduces the efficiency of LCN actuation, especially in the case of photothermal LCNs where the faster heat dissipation in water can severely limit their function. As such, LCN soft robots must be designed specifically for functioning in wet conditions, and alternative approaches such as additional methods of control should be explored. Another challenge facing the use of LCNs for aquatic soft robotics is achieving simultaneous powering and robotic function. The actuation of LCNs has been used to achieve either locomotion or control over robotic function but rarely both simultaneously. One promising approach to overcome this challenge is to decouple the mechanisms for powering and control.[14,15] Utilizing decoupled, orthogonal methods for powering and control has the potential to both solve efficiency issues when working in wet conditions and to enable more complex robotics functions.

In this work, decoupled powering and control of robotic function is achieved through the use of untethered, self-powering chemical motors paired with stimuli-responsive LCNs. The benefits of this approach are showcased in two case studies utilizing chemical motors and LCNs for small-scale mechanical devices. In the first case study, a multi-component mechanical device is fabricated that operates on the surface of water. The chemical motors provide power to a gear train, and the

transmission of this power through the gear train is controlled through the actuation of a photothermal LCN clutch gear. The second case study shows the direct integration of chemical motors onto LCN constructs through the fabrication of a milli-scale device that swims on the surface of the water. Propulsion is generated by the chemical motors, and the direction of movement is controlled through the actuation of the photochemical LCN.

The next steps in the field of aquatic soft robotics are then explored through the fabrication and characterization of a photochemical LCN that is controlled through visible light, a safer alternative to previous LCNs that rely on the use of UV light. This is enabled through the use of a custom azobenzene compound that not only undergoes isomerization in response to visible light but also has an extended *cis*-lifetime. This opens up greater possibilities for safer human interactions and eventual biomedical applications.

Chapter 2
Literature Review

2.1 Aquatic Soft Robotics

With growing interest in the development of small-scale machines and devices, there is a need for alternative powering, navigating, functioning, and control strategies that can be utilized at smaller scales.[16] The field of soft robotics, which utilizes compliant materials, has developed in response to this growing demand. The development of small-scale, soft robotics introduced new challenges for materials scientists and chemists in developing novel materials with built-in sensing, actuation, and computational abilities that can operate in complex environments.[17,18] Different materials used for soft robotics include shape memory polymers, magnetoactive elastomers, hydrogels, and liquid crystal networks.

Shape memory polymers (SMPs) are capable of deforming to one or more temporary shapes from a single fixed permanent shape. This is done by 'programming' the temporary shapes through a combination of molecular architecture and applied thermo-mechanical history.[19-22] They can deform to the programmed temporary shape(s) through exposure to external stimuli such as heat[23], light[24,25], or electricity.[26,27] SMPs are low-cost, easily processed, and often biocompatible. However, they face challenges with poor efficiency and slow response time that limits their real-world applications.[28]

Magnetoactive elastomers are soft polymers containing magnetic particles that can undergo deformations triggered by magnetic fields.[29-31] Magnetic actuation has been used to successfully achieve crawling[32], swimming[33-35], and micropump[30] devices that can operate in enclosed spaces.[36] While the magnetic response is quite fast compared to other methods of actuation[13], magneto-active elastomers are limited by the challenges of precisely and accurately distributing magnetic particles within the elastomer.[29] Additionally, the external magnetic coils required for control are typically large with high power consumption for a relatively small workspace.[13]

Among the plethora of soft robotic materials, cross-linked networks of liquid crystal polymers (called LCNs hereafter) and hydrogels have been the subject of extensive study for their many interesting characteristics.[37,38] For instance, the responsiveness of a great number of LCNs and hydrogels to external stimuli, such as heat, light, chemicals, and magnetic fields, allows for their remote control in untethered robotic applications. However, the stark dichotomy between LCNs and hydrogels in their

chemistry, biocompatibility, and more importantly, interaction with water has led the majority of scientists to favor hydrogels in developing soft actuators, robots, and devices that are sought to function in aqueous media (called “aquatic soft robotic” hereafter). The affinity of small-scale soft robots with surrounding aquatic media becomes essential in order for them to be utilized in medical procedures where the workspace is usually confined and filled with liquids, like mucus, blood, and vitreous humor.

In order to understand the dichotomy between LCNs and hydrogels it is essential to step back and scrutinize their molecular and physicochemical characteristics that pertain to soft robotics. It is also important to note a class of materials where LCNs and hydrogels seemingly confluence, namely lyotropic liquid crystal hydrogels.[39]

2.2 Materials for Aquatic Soft Robotics

2.2.1 Hydrogels

Hydrogels are soft materials that contain a significant amount of water and are composed of hydrophilic polymer chains crosslinked into three-dimensional networks via different chemical or physical interactions.[40–42] Their bioaffinity and substantial water content provide hydrogels with properties comparable to biological tissues, making them appealing for biomedical applications.[43–46] As such, hydrogels have been used in a variety of biomedical applications including biosensors, scaffolds, medical microrobots, and drug delivery systems.[47–51] Many hydrogels can absorb or lose water through a change in hydrophilicity in response to various external cues such as temperature, pH, light, electric field, or chemicals. The molecular-scale hydrophilicity change can trigger coil-to-globule transitions, resulting in reversible macroscopic deformation in the form of swelling and shrinkage (Figure 2-1). Such an actuation mechanism is driven by water uptake/release, which depends on the diffusion of water molecules into or out of the hydrogel network. In the majority of cases, hydrogel actuation is isotropic, which limits their widespread use in soft robotic applications where asymmetric shape transformations form the basis for locomotion and function. Anisotropic shape changes of hydrogels, hitherto, have been achieved via two dominant approaches.[38,40,52] First, isotropic hydrogels exposed to nonuniform external stimuli such as patterned electric or light fields, show nonuniform shape transformations.[53] In this approach, the mechanism of shape morphing at the microscale is still isotropic and the spatiotemporal control of the applied nonuniform external stimuli with high precision and resolution is challenging.[54,55] The second approach is to prepare hydrogels with intrinsic microscale anisotropy by introducing nonuniformity, heterogeneity, or gradients into their micro- and

macrostructures.[56–59] These approaches can result in relatively complex deformations of hydrogels. However, the diffusion-based shape-transformation of hydrogels is inherently slow and the obtained output work is small, presenting major roadblocks for aquatic soft robotic applications requiring fast shape changes.[40,60–63]

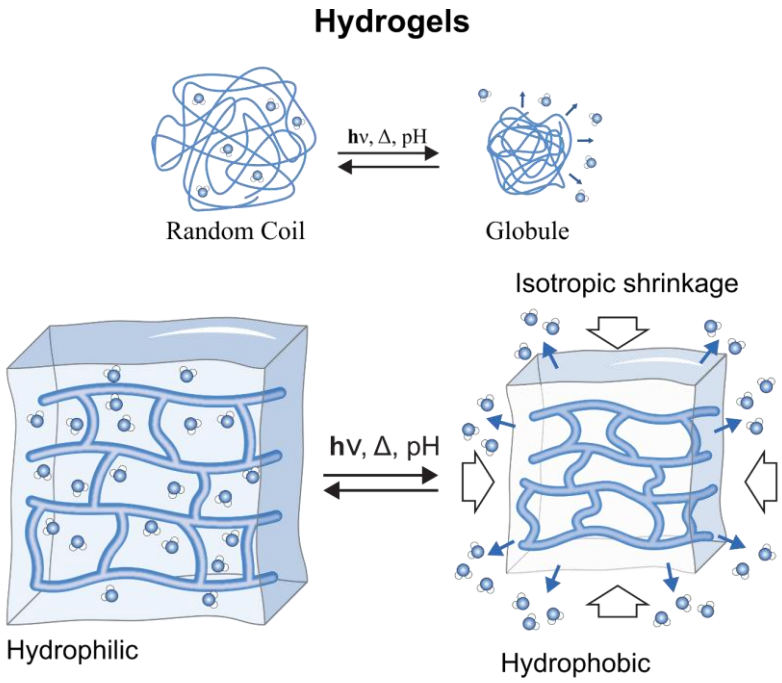


Figure 2-1 Shape change mechanism of hydrogels: external stimuli such as light, change in temperature, or change in pH causes the hydrogel network to become hydrophobic and water molecules move out of the hydrogel, resulting in isotropic shrinkage.

2.2.2 Liquid crystalline materials

Thermotropic liquid crystals (LCs) are molecules with anisotropic, typically rod-like, shapes that contain a relatively rigid core and flexible peripheral alkyl tails. The rigid core enables ordered crystalline packing which diminishes upon heating, as facilitated by the flexible tails. At a certain temperature range, the LC molecules (mesogens) can flow like liquids but have some level of orientational and/or translational order like solids.[64] The anisotropic molecular order gives rise to anisotropic physicochemical properties, such as viscosity, refractive index, dielectric constant, and

magnetic susceptibility. Liquid crystal networks (LCNs) are LC-containing polymers crosslinked into three-dimensional networks. Based on their crosslinking density, LCNs can be classified into lightly crosslinked liquid crystalline elastomers (LCEs) or highly crosslinked glassy networks. Throughout this thesis, the general term LCN will be used.[65] Crosslinking arrests the local mesogen alignment and imparts the network with anisotropic mechanical properties and response to external stimuli. Exposure to heat disturbs the arrested LC order and can lead to (in the case of LCEs) a transition between liquid crystalline and isotropic phases. For mesogens aligned in a certain direction (the director), such order-disorder transition manifests in anisotropic macroscopic shape change, which is reversible thanks to the elasticity of the polymer network.[66] Uniformly aligned domains of LCNs typically contract along their director and expand perpendicular to it (Figure 2-2). Accordingly, the shape change of two- or three-dimensional LCN constructs can be programmed by encoding predetermined director fields into LCN pixels or voxels through various techniques, such as surface alignment[67–70], photoalignment[71–79], strain[80–84], and the use of external magnetic or electric fields.[85–91]

The chemical structure of mesogens, their position inside the network, and the degree of crosslinking affect the physicomechanical and actuation properties of LCNs.[66,92,93] LCNs generally outperform hydrogels in programmability, the complexity of shape morphing, response time, and output work. Moreover, in contrast to hydrogels which are predominantly used in water, LCNs are usually utilized in dry conditions due to their limited affinity to water and the inefficiency of thermal actuation under water. LCNs have not been widely regarded as biocompatible materials, which limits their potential in biomedical applications. But, recently, a number of reports investigated their cytocompatibility,[66,94–97] as well as in-vivo animal studies.[98] For instance, Shaha et al implanted LCN constructs mimicking intervertebral discs in rats. Their histological analysis showed that LCN implants caused the development of a fibrous capsule but no obvious inflammatory response or noticeable swelling on the animal.[98] There is still a need for longitudinal studies on their effect on the human body.

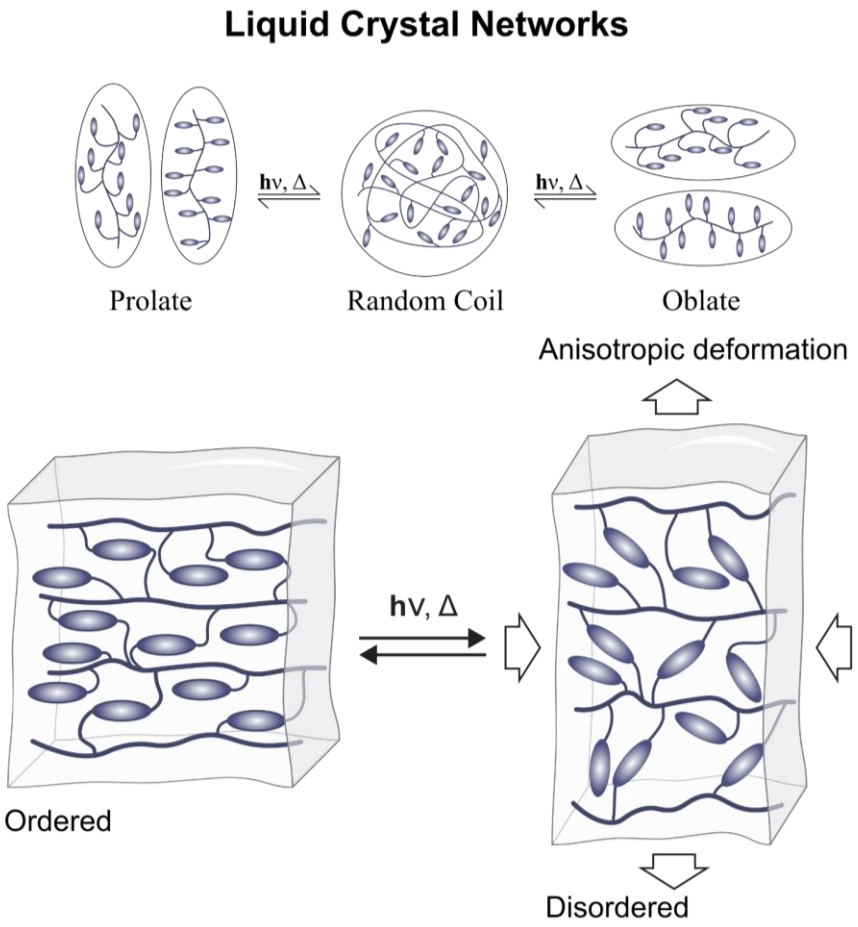


Figure 2-2 Shape change mechanism of liquid crystal networks: external stimuli such as light or heat cause a reduction in the molecular order, resulting in anisotropic deformation.

Lyotropic liquid crystals undergo phase transitions due to changes in their concentration in a solvent as well as changes in temperature. Confinement and shear have been utilized to align nematic LLCs, and like in thermotropic LCNs, the order can be frozen upon crosslinking.[39,99] Shape-morphing hydrogels of chromonic LCs have been reported in recent years with mechanisms rooted in anisotropy of network architecture and mechanical properties.[100–102] The remarkably low twisting elastic constant and the sensitivity of LLC phases to external cues such as temperature and shear make accurate on-demand molecular alignment control of LLCs and their crosslinking into ordered networks extremely

challenging.[103] For these reasons, lyotropic liquid crystal hydrogels have not yet found their way as actuators to mainstream aquatic soft robotics, despite the promise of reconciling LCNs and hydrogels.

2.3 LCNs and Water

2.3.1 LCN Actuators in Contact with Water

There has not been a report that systematically studies, in-depth, the affinity between LCN actuators and water through measurement of surface/interfacial energies, wetting, adhesion, absorption interactions, and static/dynamic contact angle measurement. The scattered knowledge on the subject is perhaps due to the diversity of LCN formulations thus far reported. A survey of the literature shows that the static contact angle of water on thermotropic LCNs varies between 60° and 100°.[72,104–108] The literature lacks information about dynamic contact angles, especially the receding contact angle, which is a better metric to determine LCNs' hydrophobicity/hydrophilicity.[104] In addition to the water contact angle, the permeability of water (or water vapor) can be used to gauge the level of hygroscopicity. The available data show that the water vapor permeability of typical liquid crystal polymers (LCPs) is significantly lower than other studied polymers, such as Nylon 6, polyethylene terephthalate (PET), and high-density polyethylene with water absorption of less than 0.04%.[109–112] In an older study, blending PET with LCPs reduced water vapor transmission by almost 90% compared to pure PET.[113] The data on the permeability of LCNs is limited. For LCNs in aquatic environments, water at different temperatures acts as either a heat source or sink regulating the actuation and relaxation driven by other stimuli, such as heat and light. Moreover, water has no considerable diffusion into or out of the majority of LCN networks. LCNs have a complicated relationship with water for they display different actuation behaviors when encountering it.

Of the LCN formulations reported in the literature, the actuation behaviour of only a limited number of them is examined in contact with water. It is shown, in all such studies, that the thermodynamic and physical interactions of LCN actuators with water affect their mode, extent, and efficiency of actuation. In some of these studies, water only thermodynamically interacts with LCNs and is essentially a means to deliver or dissipate thermal energy. In some others, the physical interaction of LCNs with water as a medium regulates their soft robotic functionality. For instance, the locomotion (consecutive cycles of actuation and relaxation) of submerged LCNs is affected by volumetric forces, such as drag and hydrodynamic forces, whereas, when the LCN is positioned at the air-water interface, surface forces such as capillary become increasingly important.

As shown in Figure 2-3, the common actuation mechanism of almost all LCNs, whether submerged or positioned at the air-water interface, is a reduction in molecular order rendered by heat or light.[71,114–118] The heat can be introduced to LCN actuators either directly through high-temperature air or fluid or indirectly through electrical current (or Joule heating) or light. The latter is known as the photothermal mechanism in which LCNs contain chemical dopants that convert absorbed light into thermal energy. Reduction of the order at the molecular scale, and shape change at the macroscale, can also be achieved through photochemical mechanisms, using molecular switches undergoing reversible isomerization reactions upon exposure to light of different wavelengths.

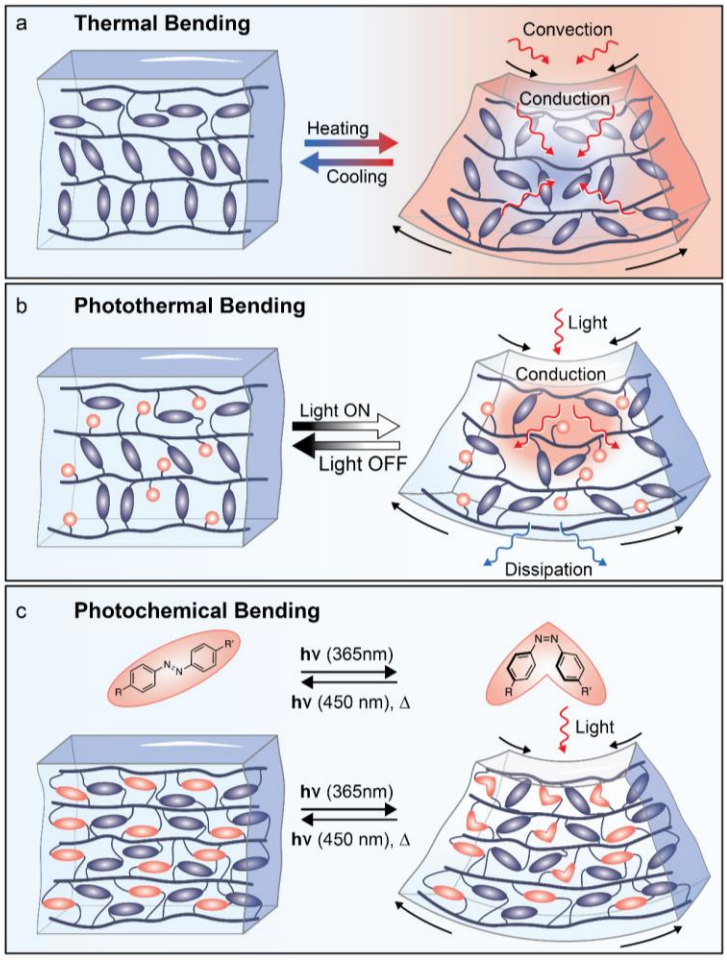


Figure 2-3 LCN Actuation Mechanisms. a) Thermally induced bending: The surrounding media is heated, typically via a convection mechanism. Conduction heating in splay aligned LCN causes a reduction in molecular order that is translated to a macroscopic shape change due to contraction/expansion at the two film surfaces; b) Photothermally induced bending: The LCN slab is exposed to light on one side. Photothermal compounds doped into the LCN convert the absorbed light energy into heat. There is conductive heating within the LCN, and the heat generated rapidly dissipates in water. The increased temperature in the LCN causes a reduction in molecular order that causes macroscopic bending; c) Photochemically induced bending: When exposed to, typically, UV light, azobenzene photoswitches in the LCN isomerize from the rod-like *trans*- to the bent *cis*-isomer. As the light is absorbed by the azobenzenes, the UV irradiation does not penetrate the full depth of the LCN slab. This results in a gradient in the *cis*-isomer population and resultant anisotropic strain and macroscopic bending. This mechanism typically does not generate heat within the sample. The blue box around the schematics demonstrates the water environment.

2.3.2 Thermal Actuation in Water

The actuation behavior of LCNs dramatically changes when they encounter water, either submerged in it or positioned at the air-water interface. The overall coefficient of heat transfer of water is immensely larger than that of air. That is, depending on the difference between the surrounding water and phase transition temperatures, warmer water can act as a superior heat source and colder water can act as a superior heat sink compared to air. The heat transfer mechanism in thermal actuation and relaxation of LCNs in dry conditions is facilitated by the typically poor conduction and (free or forced) convection of air. In contrast, water, as a heat source or sink, can trigger or facilitate thermal actuation and relaxation of LCNs by promoting molecular disorder via conformal contact (Figure 2-3a).

While the majority of LCNs used in aquatic conditions are light-responsive, some are solely thermally responsive, for which water is used as a heat source or sink. Heating and cooling of water medium are common practices in labs to produce homogeneous temperatures around LCN actuators and visually monitor their thermal deformation or measure parameters such as thermal coefficient of expansion.[73,119,120] Cold water can be used to regulate actuation and relaxation. For example, it has been found that for underwater electrothermal actuation of artificial muscles composed of liquid metal–LCN composites, higher input power is required to achieve the same actuation stroke as in air, but faster cooling in water allowed for faster relaxation.[121] The temperature gradient across a medium of warm water in contact with a cold substrate is also used to drive asymmetric underwater actuation leading to locomotion of LCN actuators.[122] Heating and cooling of LCNs by water, although seemingly easy, is impractical for aquatic soft robotic applications. The very same reason, i.e., the high overall heat transfer coefficient of water, makes it virtually impossible to rapidly alternate water temperature, which is necessary for dynamic soft actuation. Indeed, deformation driven by cyclic heating and cooling of water is extremely slow compared to photothermal or photochemical actuation.

2.3.3 Photothermal Actuation in Water

In the photothermal actuation mechanism, light absorbed by photothermal dopants locally generates heat that causes LC molecular disorder and macroscopic actuation (Figure 2-3b). Once the light source is removed the LCN relaxes back to its original shape through the dissipation of heat to its surroundings. The photothermal mechanism offers high spatiotemporal control in actuation, providing complex deformation profiles thanks to the adjustability of the spatial and temporal properties of the incident light.[71,117,123–125] In the air, photothermal actuation can be significantly faster than other stimulation

methods as it is based on heat conduction within the LCN actuator. However, the heat transfer coefficient of the surroundings dramatically affects the heat dissipation rate and shape relaxation. A crude approximation by Shahsavan et al. shows that the photothermal temperature increase of a slab of LCN upon exposure to known light intensity is much less in quiescent water than in air.[73] Indeed, the greater overall heat transfer coefficient of water makes both rates of energy storage and thermal dissipation from the LCN much faster. Accordingly, the ratio between the stored energy and the energy input, i.e., the energy conversion efficiency, is much lower. Therefore, a much higher energy input is required to create a similar photogenerated temperature increase in water than in air.

Photothermal heat generation combined with fast energy dissipation in water has created a host of possibilities to elicit aquatic soft robotic functions from LCNs. In the majority of reports, doping LCNs with organic compounds such as fast-switching azobenzene derivatives like DR1, render photothermal actuation without disturbing the director fields.[72,73,123,126] Nanoparticles have also been employed as efficient photothermal dopants that deliver selective absorption of light at different wavelengths ranging from visible to infrared. Such nanoparticles include but are not limited to, carbon nanotubes (CNTs), gold nanorods (GNRs), and graphene.[127–130] A variety of photothermal deformation profiles such as twisting, bending, coiling, and winding, upon NIR irradiation in water, are reported.[130] The use of nanoparticles to induce photothermal actuation underwater, although effective, might disturb the molecular alignment and change the mechanical properties of LCN actuators, which could adversely affect their actuation amplitude and ability to overcome drag during undulating deformations. Instead, improved photothermal functionality can be achieved by coating LCNs with photothermal materials such as polydopamine (PDA), which not only offer photostable performance and strong absorbance in the NIR region but also have a negligible effect on the mechanical properties of the LCN.[131,132]

The hydrophobic nature of LCNs can be utilized to create photothermal soft robotic locomotion and function at the air-water interface. One of the first swimming LCNs, reported by Camacho-Lopez et al., was indeed using a hybrid mechanism to slide at the air–water interface. In this seminal work, the LCN flaps deformed photothermally, bulged the capillary line, and broke the symmetry. They swam away from constant light through the thermal Marangoni mechanism, in a manner analogous to that of a flatfish (Figure 2-4a).[133] Aside from the thermal Marangoni effect that could facilitate the sliding of photothermal LCNs at the air–water interface, modulation of capillary forces acting on the contact line, although difficult, can create interesting soft robotic scenarios. For instance, the exposure of the air-facing side of LCN actuators to undulating light can be used for freeform locomotion and navigation

of LCNs on the water surface (Figure 2-4b).[134] The capillary bridge in these works is not broken and elastocapillary forces at the interface assist the relaxation stroke and better locomotion

Photothermal soft robotic locomotion and function for LCNs submerged in water present other challenges. Depending on the size of the LCN constructs and the Reynolds number of the water surrounding them, hydrostatic pressure and drag forces could suppress the deformation through fast dissipation of energy. One intuitive approach to overcome this problem is to simply increase the intensity of the incident light to create a high local temperature where the robot needs to function. For example, Martella et al. used photothermal LCN-based photonic micro-hands that can selectively grab small particles based on their optical properties.[126] The micro-hand could distinguish between particles of different colors and function selectively based on absorbance at a specific wavelength. The dark objects absorbed the incident laser and increased the local temperature, causing the LCN hand to bend. The light hitting the micro-hand with low-absorbing objects did not create sufficiently large heat to cause bending. As the microhand relaxed faster underwater than in the air, the excitation power required for actuation was five times higher.

To overcome the limitations imposed by the fast heat dissipation, drag, and hydrostatic pressure underwater, Shahsavan et al. used liquid crystal gels (LCGs) by doping LCNs with extensive amounts of short-chain mesogens like 5CB.[73] LCGs showed significantly reduced stiffness and phase transition temperature, as well as a photoinduced reduction in their density, which collectively resulted in greater actuation at the same light intensity compared to their LCN counterparts. Underwater crawling, walking, and jumping was observed for LCGs under much lower illumination intensities. However, more subtle spatiotemporal control over illumination was required to overcome the drag force and hydrostatic pressure to propel the LCG robot in an upward swimming motion (Figure 2-4c). Softening, reducing the transition temperature, and fine-tuned spatiotemporal control over the illumination were used to elicit soft robotic functions beyond locomotion. In another work, LCN films exposed to light contracted along their long axis with a slight upward bending. When the light was off the LCNs recovered to the initial flat shape. By varying the location and the size of the exposed area, different bending patterns were achieved. Cycling the light exposure on and off caused the LCN film to undergo repeated actuation, generating a propulsive force that pushes the film forward inside the water (Figure 2-4d).[80]

Deng et al. have recently demonstrated autonomous microfluidic pumping, translocation of micro-object through liquid propulsion, and hydrodynamic coupling between two non-equilibrium artificial cilia, all driven by the self-shadowing effect.[117,135] The LCN strips in their report progressively bent with elevating laser intensity in an aqueous environment, and eventually, a self-sustained oscillatory motion was realized. By implementing two orthogonal laser beams on a single specimen, the motion symmetry was broken, and programmable non-reciprocal strokes could be induced, which, in turn, affected the fluidic pumping efficiency.

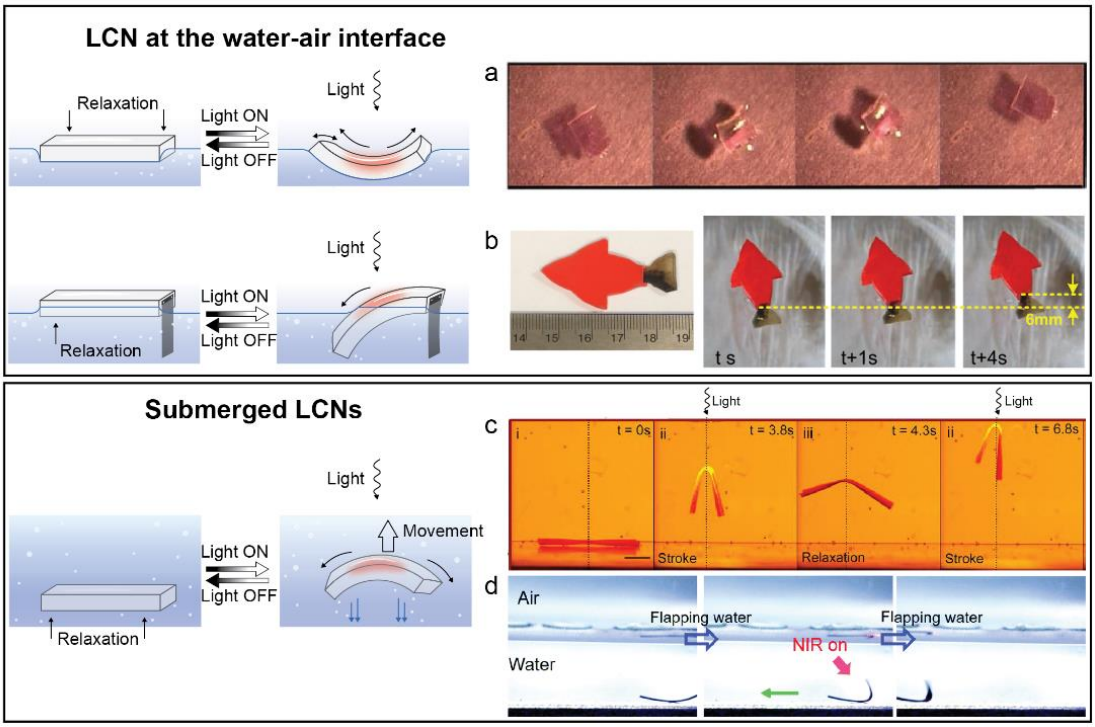


Figure 2-4 Movement of photothermal LCNs at the air-water interface and submerged in water. a) Bending of the LCN is used to manipulate the capillary line, breaking the symmetry and creating a propulsive force through the thermal Marangoni mechanism. Reproduced with permission.[133] 2004, Nature Publishing Group; b) Repeated actuation without breaking the contact line is used to generate a propulsive force that pushes the swimmer forward. Reproduced with permission.[132] 2018, American Chemical Society; c) Repeated rapid bending followed by slower relaxation through the cycling of UV light on and off is used to achieve propulsive force to achieve upward swimming. Reproduced with permission.[73] 2020, National Academy of Sciences; d) Repeated actuation of one end of the LCN through NIR light exposure is used to generate a propulsive force that pushes the LCN along a submerged surface. Reproduced with permission.[80] 2022, Royal Society of Chemistry.

2.3.4 Photochemical Actuation in Water

The photochemical effect in LCNs is often introduced by azobenzene photoswitches that undergo isomerization and induce macroscopic shape change incorporated into the LCN. Azobenzene derivatives transition from the stable rod-like *trans*-isomer into a metastable bent *cis*-isomer under

irradiation with typically UV light. The *trans*-to–*cis* photoisomerization can disrupt the polymer network and cause a decrease in liquid crystal order, which in turn can give rise to macroscopic deformation. The thermodynamically stable *trans*-isomer can be retained either through thermal relaxation or upon exposure to light in the *cis*-isomer's absorption band, typically in the blue–green region of the visible spectrum (Figure 3-2c).[136] Azobenzene derivatives with long *cis*-lifetimes and those that can be addressed with visible light have also been synthesized, due to their potential in biomedical and photopharmacological applications.[137–140] However, few of them have been incorporated into LCNs. The meta-stable *cis*-state allows for an additional level of control over the photochemically driven LCNs compared to their photothermal counterparts as the actuator remains bent for a period set by the *cis*-lifetime once the light has been removed.[141]] However, photochemical LCNs with azobenzene derivatives usually rely on UV light for actuation, which limits their potential use, especially in biomedical applications.

Many researchers have circumvented the issue of fast dissipation of photothermal heat in water by using photochemically responsive LCNs. Photochemical actuation, at its best design, is an isothermal process and hence well suited for use in water. The higher heat dissipation in water can extend the lifetime of the meta-stable *cis*-isomer as it reduces potential heat-promoted back relaxation, which in some cases has resulted in marginally larger actuation upon irradiation underwater.[142–144] Photoisomerization of azobenzene derivatives can also result in a reduction of LCN density, which can be a useful attribute when designing aquatic soft robots and locomotors.[75]

Da Cunha et al. systematically studied the contribution and role of photochemical and photothermal mechanisms in the actuation of LCNs in contact with water. LCNs with mono- and bifunctional azobenzenes with long cis-lifetimes had different underwater actuation behavior than azobenzenes with shorter cis-lifetimes, which drive photothermal rather than photochemical actuation. Under identical illumination conditions, the photochemical mechanism resulted in remarkable bending underwater, while the photothermal mechanism led to limited actuation, as expected based on the fast heat dissipation discussed earlier. The fast dissipation of heat in water stymied the relaxation of LCNs which typically rely on thermal back relaxation in photochemical mechanisms. An amphibious walker prepared from photothermal LCNs could consequently move in water at a slower speed.[145]

The slow relaxation of photochemically active LCNs enables on-demand manipulation of the capillary line when they are positioned at the air–water interface. For example, Hu et al. used

optocapillarity induced by the deformation of LCNs at the air–water interface to achieve programmable and reconfigurable two-dimensional assemblies.[146] UV irradiation induced directional bending in the film, which was used to obtain curvature of menisci at the edges of the actuators, providing control over the magnitude and direction of the attractive or repulsive capillary forces between the actuators. Different assembly patterns were achieved through different combinations of upward and downward bending of the actuators (Figure 2-5a). Bilayers of LCNs and other materials have also been used to construct soft robots capable of swimming at the air–water interface. Ma et al., for instance, fabricated a bimorph composite swimmer consisting of an LCN film and a Kapton film. The actuation was controlled through exposure to UV, with fast relaxation when exposure ceased. The deformation was attributed to continuous cycling between the *trans* and *cis* isomers of the azobenzene rather than the *trans–cis* isomer ratio. By cycling the UV light, the swimmer propelled itself forward with downward beats into the water, analogous to how dolphins swim (Figure 2-5b).[147]

Swimming underwater solely based on the photochemical deformation of LCNs has rarely been reported. The only successful photochemical swimmer is reported by Huang et al. through operating the swimmer via periodic exposure to UV and white light, creating an artificial flagellum swinging back and forth and pushing the LCN construct forward (Figure 2-5c). Given the slow nature of photochemical deformation, the speed of locomotion was very low.[14] While photochemical LCNs have not shown much utility as swimmers up to date, their slow actuation and relaxation have been the basis of design for the manipulation of water itself or other objects underwater. Van Oosten's well-known work is an example of photochemically driven LCNs that function like cilia underwater.[148] The photochemically driven artificial cilia were used as mixers or pumps, capable of both forward and backward strokes. Asymmetric movement of the cilia was achieved by using two different azobenzene dyes, varying the composition of the actuator in-plane and allowing for different degrees of bending based on the color composition of light used. Later on, photochemical light-tracking fiber assays resembling cilia were reported with the potential for the transport of submerged objects.[144,149] A more sophisticated design inspired by aquatic polyps was later developed by da Cunha et al. using a hybrid construct of photochemical LCNs and passive magnetic elastomers to grasp and release buoyant objects underwater on demand (Figure 2-5d).[15] In addition to swimming and cargo transport, photochemical LCNs as confining surrounding media have been used to transport and mix liquids.[150–152].

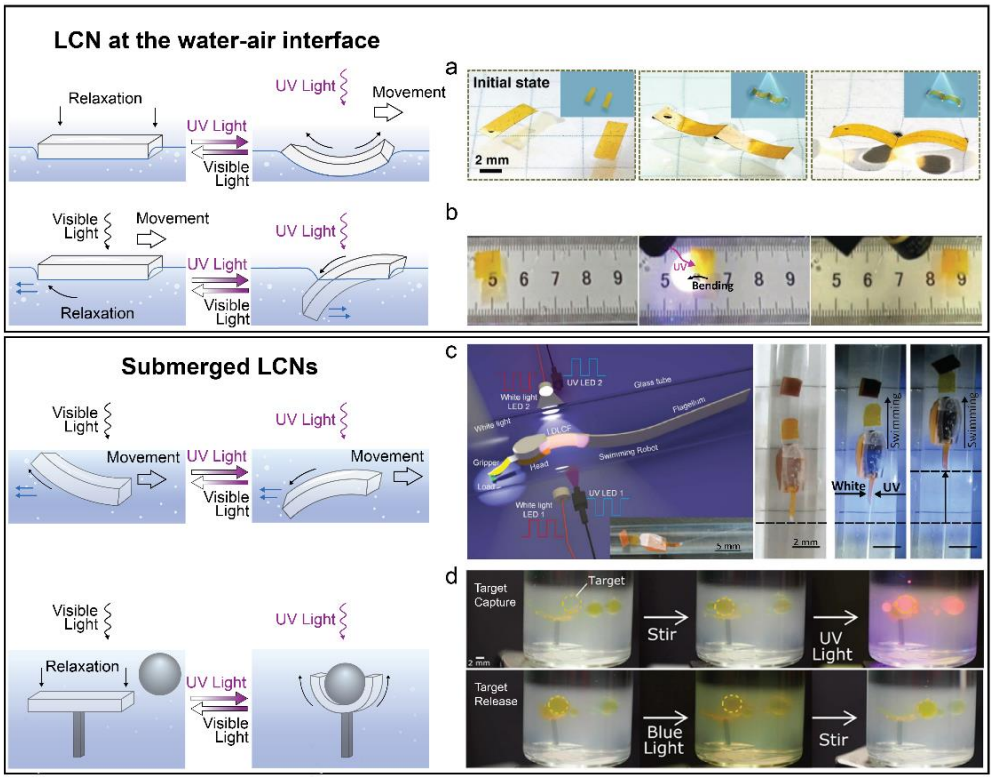


Figure 2-5 Movement of photochemical LCNs at the air–water interface and submerged in water. a) Directional bending of the LCN creates a curvature of the menisci at the edges of the actuators, resulting in controllable attractive or repulsive capillary forces between the actuators. Reproduced with permission.[146] 2020, Springer US; b) Repeated downward actuation that breaks the capillary line with fast relaxation generates a propulsive force that drives the LCN swimmer forward. Reproduced with permission.[147] 2019, Wiley; c) Bending of the LCN through periodic exposure to UV and white light causes an artificial flagellum to swing back and forth, which generates a propulsive force that pushes the swimmer forward. Reproduced with permission.[14] 2015, Springer Nature; d) LCN grippers bend to grasp and relax to release buoyant targets through exposure to UV and visible light, respectively. Reproduced with permission.[15] 2020, National Academy of Sciences.

LCNs exhibit entirely different actuation behavior in wet and dry conditions. While water appears to be a good heat source, it can be practically utilized in soft robotic applications only as a heat sink as it facilitates the dissipative relaxation of thermally responsive LCNs. Particularly, photothermally driven LCNs, which enjoy precise spatiotemporal control over their actuation, can take advantage of water's high overall coefficient of heat transfer for their rapid relaxation, and as such are far more widely studied. But photothermal actuation underwater or at its interface with air comes at the cost of high

energy input for the actuation and low overall energy efficiency. Despite the relatively higher efficiency of the photochemical actuation mechanism in water, photochemically driven LCNs often rely on the use of UV rather than visible light, limiting their potential applications, especially in biomedical fields. In addition, both photochemical and photothermal actuation of LCNs are significantly affected by capillary, hydrostatic, and drag forces exerted on them by water. For small-scale robotics, the problem of locomotion at low Reynolds numbers also adds up.[153]

2.3.5 Research Objective

LCN actuators have shown potential as building blocks of soft and small-scale robots to be operated in flooded terrains, thanks to their inherent programmable, anisotropic, and stimuli-responsive properties, which hydrogels often do not inherently have. There exists a considerable body of literature demonstrating proof-of-concept aquatic soft robotic locomotion or functions driven by LCN actuators. However, they have not yet found practical real-world applications. This issue is arguably rooted in the complicated nature of the interaction between LCNs and water. As mentioned earlier, a powerful approach to enhance the efficiency of LCNs in aquatic and medical soft robotics is to decouple soft robots' locomotion from their function by utilizing orthogonal mechanisms. For this, LCNs can be equipped with responses to other stimuli such as magnetic fields. The incorporation of magnetic particles in LCN films has been recently used to achieve their magnetically controlled locomotion which was decoupled from their underwater photochemical or photothermal function.[15,154,155] However, the doping of LCNs with microparticles interferes with their molecular alignment making necessary a trade-off between LCN performance and particle loading. Alternatively, a second mechanism for locomotion can be introduced, such as chemically-driven propulsion for self-powering. Self-powered mechanisms such as chemical motors are of particular interest because they can operate autonomously by consuming onboard or in-media chemical fuel. Among these, Marangoni motors are a popular choice for locomotion at the air–water interface. This motor mechanism (inspired by the locomotion of semiaquatic insects)[156] relies on propulsive forces generated by anisotropic surface tension gradients,[157] and it has been exploited to propel robotic platforms locomoting on the surface of water.[158,159] Many approaches in developing Marangoni-propelled systems hinge on chemical fuels added at the air–water interface or trapped and released from a motor matrix. These motors have evolved from microdroplets[160] to systems using organic matrices[158,161,162] and fluid reservoirs[159,163], with greater capacity for fuel storage. While these systems usually present control and efficiency challenges, they can provide sustained propulsion over long periods without the need for continuous

external stimuli. Crucially, the use of such chemical motors provides power without interfering with the molecular alignment, and therefore function, of LCNs. This opens up new possibilities in the fabrication and operation of small-scale devices fabricated from LCNs.

In this work, we demonstrate the power and potential applications of decoupling locomotion from robotic function for small-scale devices through two case studies using untethered, self-powering chemical motors and stimuli-responsive LCNs tailored for use in wet conditions. An LCN is also designed to enable safer interaction with people, looking forward to potential biomedical applications.

First, a photothermal LCN designed for improved actuation efficiency when in contact with water is used in conjunction with chemical motors for a milli-scale, multi-component mechanical device that operates on the surface of water. The second case study directly integrates chemical motors onto a photochemical LCN swimmer, wherein the chemical motors provide propulsion and the LCN swimmer is selectively actuated for directional control. In both of these case studies, the use of UV light is required for actuation, which limits potential biomedical applications. For the final part of this work, a novel azobenzene compound that undergoes *trans-to-cis* isomerization under visible light is used to fabricate a photochemical LCN that doesn't require the use of UV light.

Chapter 3
Plasticized Liquid Crystal Networks and Chemical Motors

3.1 Introduction

Stimuli-responsive cross-linked networks of liquid crystal polymers (LCNs) offer interesting solutions for the control of robotic systems by inducing localized actuation. The sensitivity of these materials to a variety of cues, such as light and temperature, and their shape-change programmability, through different molecular alignment methods, have triggered a great body of research into their potential applications in soft robotics.[64,125,164–169] The majority of reported LCN systems rely on direct heat or photothermal heat generation for actuation. However, these methods typically have lower energy conversion efficiency due to the large energy loss from heat dissipation to the surroundings. The actuation is even less efficient, and consequently slower, under or at the surface of the water which has a high overall coefficient of heat transfer. As demonstrated in previous work, the addition of a nematogenic solvent to the LCN can sharpen the nematic to isotropic transition temperature (T_{NI}), decrease the energy required for the actuation, and enhance the actuation efficiency to a point where the system can change its shape underwater.[73] For a similar reason, the photothermal actuation of LCNs plasticized with short-chain nematogenic solvents (PLCNs) was selected for achieving large deformations in wet conditions.

This work is the first of two case studies included in this thesis demonstrating the performance of protein motors and shape morphing LCNs as orthogonal mechanisms for untethered powering and control of a small-scale device. In this case study, their use for the powering and control of a milli-scale, multi-component mechanical device is explored. We designed and fabricated a milli-scale powertrain transmission with active gears that integrate motor and clutch functionalities into the device (Figure 3-1). The active driving gear uses Marangoni propulsive forces at the air–liquid interface generated by onboard protein motors.[158] The active clutch gear uses photothermal actuation of PLCNs to bend the gear teeth and disengage from the gear train,[73] breaking the transmission across the gear train. While Marangoni self-powered motors and untethered control of LCNs have previously been studied separately, the integration of the two mechanisms allows for simultaneous powering of the gear train and orthogonal untethered control of the transmission, which offers new design and control possibilities for multi-component and multi-functional mechanical devices and soft micromachines.

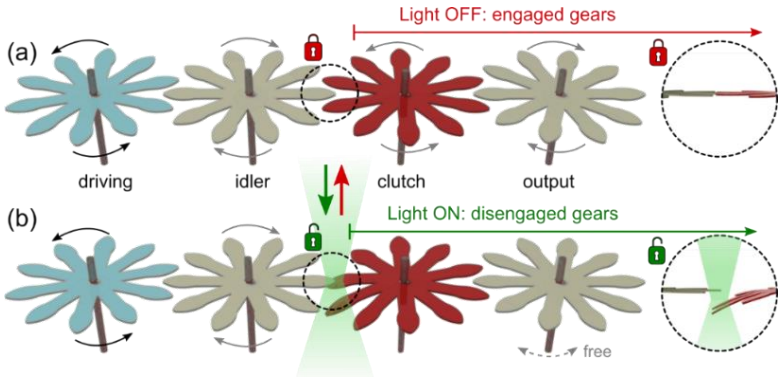


Figure 3-1 Concept of the powertrain transmission consisting in a gear train with active gears. The driving gear powers the gear train via onboard chemical motors. The clutch gear, fabricated from PLCNs, is photothermally activated to a) engage and b) disengage from the gear train.

3.2 Materials & Methods

3.2.1 Materials

Bi-functional monomer 1,4-bis-[4-(6-acryloyloxyhexyloxy) benzoyloxy]-2-methylbenzene (M1), mono-functional monomer 4-(6-acryloxy-hex-1-yl-oxy)-phenyl 4-(hexyloxy)-benzoate (M2), and low molecular weight non-reactive liquid crystal 4-cyano-40-n-pentylbiphenyl (5CB) were purchased from SYNTHON Chemicals GmbH & Co. KG.

Dispersed red 1 acrylate (DR1A), 2,2-dimethoxy-2-phenylacetophenone (Irgacure 651) N,Ndimethylformamide (DMF), 1,1,1,3,3,3-hexafluoro-2-propanol (HFIP), and crystal violet dye were purchased from Sigma-Aldrich. Brilliant yellow (BY) was purchased from TCI. Polyimide SE-1211 was donated by Nissan Chemical Industries. All reagents and solvents were used as received without further purification. Squid sucker ring teeth (SRT) proteins were extracted from Loligo Vulgaris squid species and purified as described elsewhere.[171]

3.2.2 Gear Train Fabrication

The driving and idler gears were fabricated from polyethylene terephthalate (PET) films (100 mm thick). The PET films were laser-micromachined to the desired gear design. G21 syringe needles were adhered to the bottom of a polystyrene Petri dish and served as vertical axles. The Petri dish was filled with deionized water and the gears were assembled floating at the air–liquid interface. The driving gear was partially coated on the edges of its teeth with a solution of purified SRT protein dissolved in

hexafluoroisopropanol (HFIP) at a concentration of 50 mg mL^{-1} (with an additional 1% crystal violet dye for visualization). Coated gears were dried in a fume hood for 1 h. Finally, the performance of the motors and the gear train was recorded with a Sony HDR camera (25 fps), and velocities were analyzed in MATLAB with a custom particle-tracking code.

3.2.3 Fabrication and Characterization of LC-Based Gears

The LCN films were fabricated by injecting a mixture of M1 and M2 monomers into capillary cells (100 µm gap) with predetermined molecular alignment at temperatures higher than the mixture clearing point (T_{NI}). The mixture was cooled down to its nematic mesophase at 30 °C ($<T_{NI}$); afterward, it was cross-linked by photo-polymerization using UV light. Plasticized LCNs (PLCNs) were made by adding 15 wt% 5CB to the initial mixture. LCN and PLCN films were micromachined to the desired gear shape using an LPKF ProtoLaser U3 laser cutter (3.5 W, 54 kHz). Further details of the fabrication and molecular alignment procedures can be found in Section 3.3.2. The assembly of the fabricated LCN and PLCN gears into the gear train was similar to the process stated in the section above.

3.2.4 Materials Characterization

Glass transition and nematic-to-isotropic temperatures (T_g, and T_{NI}) of the polymerized LCN and PLCN films were measured by differential scanning calorimetry (DSC) using a DSC2500 from TA Instruments. The variation of heat flux with temperature was monitored for LCN and PLCN samples between 80 °C and 150 °C in two consecutive cycles (10 °C min^{-1}). Driving gears were analyzed by Fourier Transform Infrared (FTIR) spectroscopy in a ThermoFisher Nicolet iS20 spectrometer with an Attenuated Total Reflection accessory at 128 scans and 4 cm^{-1} resolution per spectrum.

3.2.5 Actuation Characterization

To estimate the photothermal actuation of LCN and PLCN gear teeth, we used LCN and PLCN cantilevers with splay alignment. The length of each cantilever was set to 6 mm, corresponding to the length of each gear tooth from its tip to the center of the gear. One-end fixed cantilevers were exposed to light from a high-pressure mercury vapor short arc UV lamp (Omnicure S2000, Excelitas Technologies) with distinctive peaks in the UV-vis region (300 nm to 600 nm). The tip displacement vs. light intensity was monitored by a digital microscope (Dino-lite) and measured manually using the Fiji image-processing package.

3.3 Results & Discussion

3.3.1 Protein Motors for Power Generation[1]

To power the gear train, we applied a functional motor coating to an initially inactive gear and used it as the driving gear in our transmission system. The motors are based on Marangoni propulsion achieved by the release of hexafluoroisopropanol (HFIP) stored in squid sucker ring teeth (SRT) proteins.[158] HFIP is a volatile low surface tension solvent that is used as a chemical fuel entrapped in an SRT protein motor matrix,[170] which is composed of semicrystalline polypeptides found in suction cups on the tentacles and arms of squids.[171,172] SRT proteins can be dissolved in HFIP, resulting in a motor-and-fuel complex solution that can be applied as a coating to a broad range of substrates and materials (in this case, the teeth of the driving gear, Figure 3-2a).[173,174] After evaporation of the solvent, residual fuel remains infused in the SRT protein coating. As the coating comes in contact with water the fuel molecules infused in the protein matrix diffuse into the water and lower the local surface tension.

We fabricated a module 1 (m1) gear set with 10, 20, and 30 teeth (z10, z20, and z30 respectively) (Figure 3-2b) and applied the protein motor coating to the teeth. The gears were designed with a modified extended teeth profile to increase the cantilever length and facilitate fuel release and the clutch function. By selectively coating one side of each tooth, we can create an anisotropic surface tension gradient around the gear tooth that generates a Marangoni propulsive force towards high surface tension. This results in the Marangoni-driven rotation of an active gear rotating on a fixed axle, which constrains translational motion and enforces rotation. We can preprogram rotational motion in clockwise (CW) or counterclockwise (CCW) directions by selectively coating either side of the gear teeth (Figure 3-2c and d), and the fuel can be reapplied as needed. Fourier Transform Infrared (FTIR) spectroscopy analysis of the motor-coated gear teeth showed characteristic absorption bands from the protein (amide I, amide II, amide A), fuel (1100–1300 cm^{-1}), and the polymer substrate (polyethylene terephthalate PET film, 1700–1800 cm^{-1}, 2800–300 cm^{-1}), which indicates that the protein motors are successfully integrated with the gear teeth while conserving the infused fuel (Figure 3-2b).

[1] Completed by collaborators, Bioinspired Materials Lab at the University of Michigan

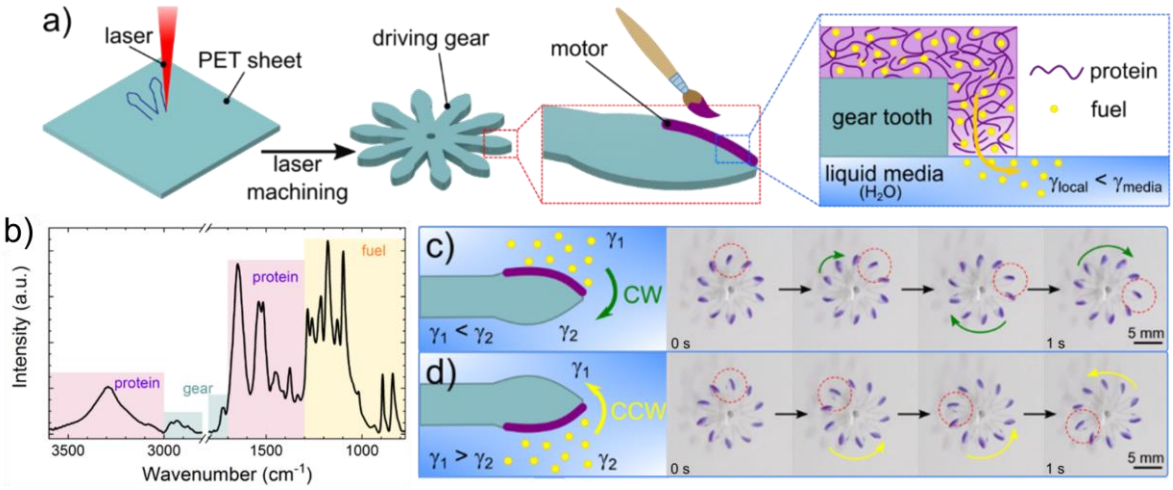


Figure 3-2 Protein motors. a) Fabrication of the driving gear by laser micromachining of PET thin sheets and application of functional motor coating consisting of chemical fuel entrapped in a protein matrix; b) chemical analysis of motors in driving gear by FTIR; c) clockwise (CW) and d) counterclockwise (CCW) motion of the driving gear by selective motor coating application on either side of the teeth.

The motor coating can propel the gears with rotational velocities up to 150, 47, and 45 rpm for z10, z20, and z30 teeth, respectively (Figure 3-3). As the fuel is released into the water surface and is progressively depleted from the motor matrix, the velocity decreases accordingly due to a lower local concentration of chemical fuel at the interface. Due to the high efficiency of the motors, the gear train can be powered with very small amounts of fuel and can operate for prolonged periods of time with a single coating application (up to 20 minutes), which makes the material very attractive as a modular power source for the driving gear.

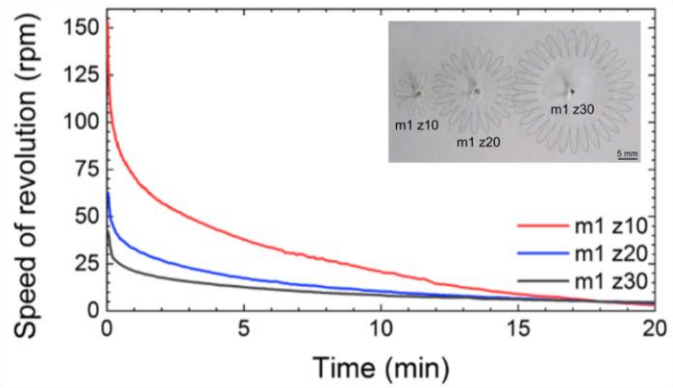


Figure 3-3 Rotational speed of m1 driving gears (z10, z20, and z30).

3.3.2 Liquid Crystal Network Clutch Fabrication

To design and fabricate a stimuli-responsive active clutch gear, we chose acrylate-based glassy liquid crystal networks due to their propensity for accurate, yet straightforward molecular alignment. The selected liquid crystal networks are aligned using photoalignment; a powerful tool for the precise alignment of liquid crystals due to its accuracy and versatility.[64] Complex alignment patterns can be achieved using linearly polarized light and patterned photomasks.[71] As shown in Figure 3-4a, the LCN is composed of a mesogenic diacrylate monomer as a cross-linker (M1: 7.7 mol%), side-chain mesogenic mono-acrylate monomers that form the backbone (M2: 90.3 mol%), and mono-acrylate photo-chromophore molecules (DR1A: 1 mol%) for photothermal local heat generation. Irgacure 651 (1 mol%) was used as the photoinitiator. According to the design in Figure 3-1, the gear teeth on the LC-based clutch must be able to undergo reversible and on-demand bending actuation. We can achieve such a shape change by a splay alignment of mesogens through the thickness of an LC-based construct. As shown in Figure 3-4b, a splay LCN film exposed to photothermal heating bends due to expansion on the side with homeotropic alignment, and shrinkage on the opposing side with planar alignment.

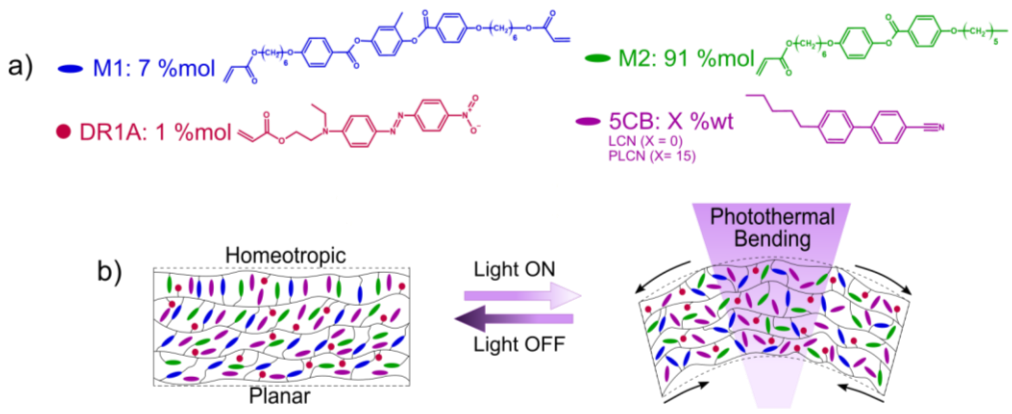


Figure 3-4 a) Molecular structure of constituent molecules in LCN and PLCN; b) mechanism of photothermal bending deformation in LC-based crosslinked networks.

In order to render a similar shape-change behavior on the teeth of the LCN clutch gears, we aligned the mesogens on one side of the film radially and aligned them homeotropically on the other side. Figure 3-5 shows a schematic view of the LCN gear fabrication process through the conventional capillary filling of an empty glass cell. We chose a photoalignment technique to induce in-plane radial orientation of mesogens adjacent to one side of the cell. For this, we spin-coated a glass substrate with a brilliant yellow and dimethylformamide (BY-DMF) solution, baked it at 90 °C, and exposed the substrate to blue light ($\lambda \sim 447$ nm) through a polarization mask. Our polarization mask was made of multiple polarizers cut into wedges using a laser micromachining tool. They were then assembled manually on a glass substrate to form a circular mask with azimuthal polarization. The BY molecules exposed to the light with azimuthal polarization render an orthogonal LC molecular alignment. The homeotropic molecular alignment on the opposing side was achieved by coating the substrate with polyimide. After cross-linking of the LC mixture by UV, a typical fan texture of the transmitted light through the fabricated film between crossed polarizers confirmed the successful radial alignment of the mesogens. The cross-linked film with radial and homeotropic molecular alignment on opposing sides was then laser micromachined into the desired gear shape. Afterward, the gear was suspended on the air–liquid interface for further experiments.

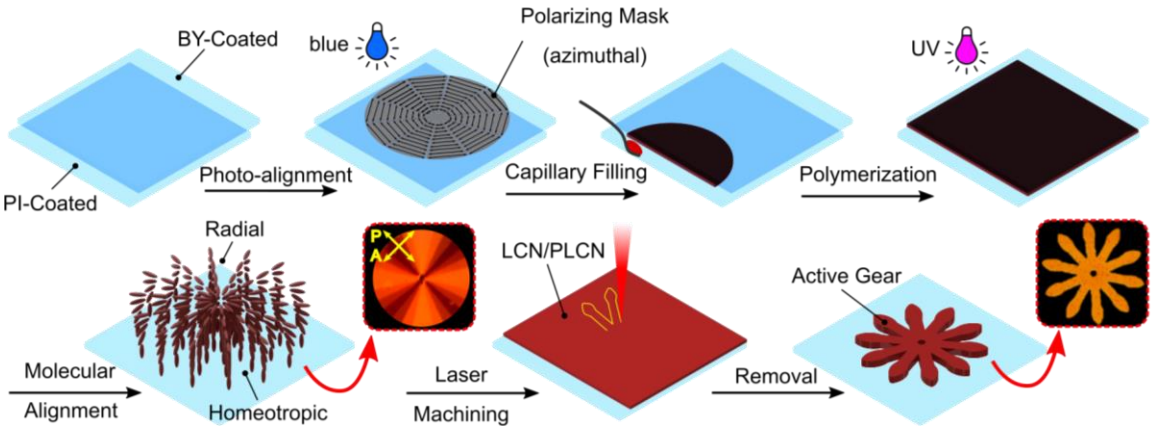


Figure 3-5 Fabrication schematic view of the LCN gears fabrication with pre-determined molecular alignment. Molecules are aligned radially adjacent to the side of the cell that is exposed to polarized light. Molecules are aligned homeotropically on the other side of the film.

3.3.3 Liquid Crystal Network Clutch Characterization

Initial experiments on the photothermal actuation of LCN gears at the air–liquid interface did not result in a discernible shape-change of gear teeth as desired (Figure 3-6a). We postulate that the photothermal actuation of the LCN gear is hindered mainly due to the extensive dissipation of generated heat from the bottom side that is exposed to the water. Consequently, the bending actuation of the gear teeth is not large enough to overcome the capillary forces acting on them. It has been recently shown, in a similar scenario, that the energy conversion efficiency and thermal actuation of photothermal LCNs dramatically decrease when they are immersed in water.[73] Such a reduction was partly attributed to the extensive dissipation of generated heat inside water, and partly to the drag force acting on the LCN construct.[73] Plasticizing the original LCN network by adding low molecular weight liquid crystal molecules, such as 5CB, was proposed as a solution to alleviate this problem. We added 15 wt% 5CB to the LCN precursor to plasticize the network and facilitate its photothermal deformation at the air–liquid interface. Our initial assessment of the thermo-physical properties using differential scanning calorimetry (DSC) showed that the glass transition temperature (T_g) of the plasticized LCN (PLCN) is greatly reduced compared to that of its LCN counterpart. Figure 3-6b shows the results of the second thermal cycle after erasing the thermal-memory of the samples in the first cycle. Both samples do not show an appreciable nematic-to-isotropic transition, which is expected due to the supercritical nature

of phase transition for this class of glassy networks.[175] For this class of materials, shape change occurs gradually as the LCNs are heated beyond their T_g. The glass transition temperature of the PLCN (T_g ~ 4.5 °C) is reduced compared to that of the original LCN (T_g ~ 9.5 °C), which widens the thermal actuation window by almost 14 °C. In previous work, it was observed that LCNs become remarkably softer by the addition of a nematogenic solvent to their precursor.[73] We anticipate higher energy conversion efficiency as a result of the decrease in the T_g and stiffness. Indeed, the plasticization of the LCN resulted in more efficient photothermal actuation of gear teeth, allowing the gear to break the surface tension and submerge in water by bending (Figure 3-6c). The photothermal actuation of splay cantilevers in air, shown in Figure 3-6d, demonstrates the great improvement of bending vs. light intensity for PLCN samples. Initially, the clutch gear was positioned such that the teeth would actuate upwards into the air to disengage from the neighboring gear (homeotropic side facing the water). However, the PLCN was unable to overcome the surface tension and elastocapillary forces acting upon it. As such, the configuration was modified so the teeth would instead actuate downwards into the water (homeotropic side facing air). The PLCN is not hydrophobic, as determined by its contact angle with water (<90°). By actuating into the water, the PLCN has to overcome a lower force and is able to successfully break the surface tension and actuate into the water.

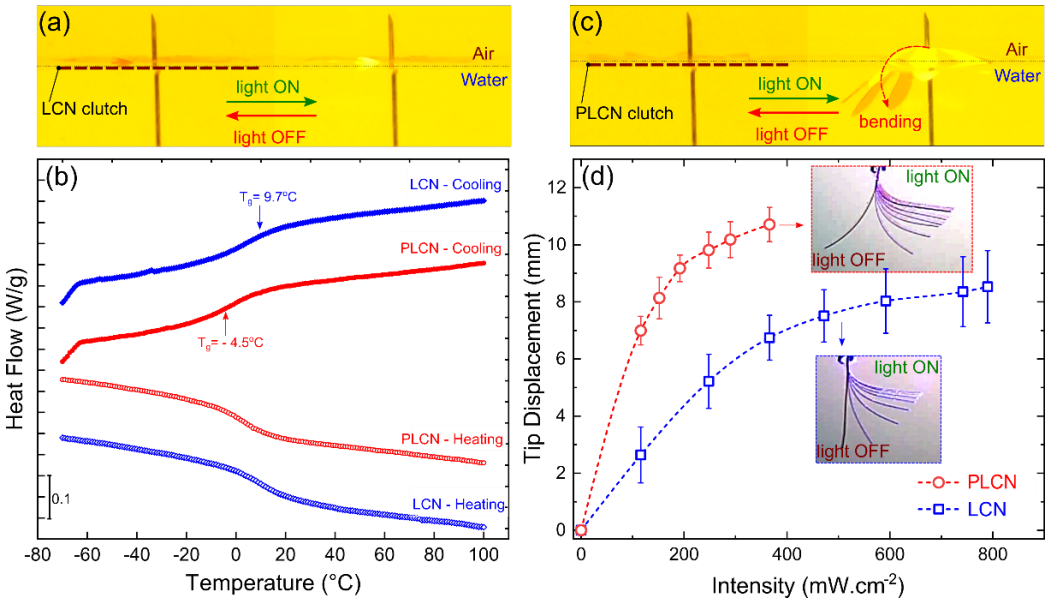


Figure 3-6 a) Exposing LCN gears to light with high intensities did not lead to breaking of the capillary bridge; b) DSC results from 70°C to 100°C shows the large shift of the glass transition temperature by adding 15 wt% 5CB to the original LCN mixture; c) PLCN gear underwent a drastic shape change with even lower energy input due to the lower Tg and stiffness, breaking the surface tension and bending into water; d) the difference between the photothermal deformation of LCN and PLCN cantilevers in air.

3.3.4 Orthogonal Actuation of a Hybrid Gear Train Mechanical Device[2]

To demonstrate the active control of power transmission by the two orthogonal signals of chemical energy and light, we integrated active gears into a milli-scale proof-of-concept gear train (Figure 3-7). The gear train consists of the (i) driving gear (with a chemical motor coating), (ii) idler gear, and (iii) clutch gear (PLCN). The driving gear was selectively coated with protein motors to generate Marangoni propulsive forces as previously discussed. The protein motors, visible in dark violet color, were selectively applied on one side of the gear teeth only, inducing counterclockwise (CCW) rotation on the driving gear. The rotational motion is transmitted to the adjacent idler gear (CW), and then to the clutch gear (CCW), which can be observed by tracking marks on the surface of the gear teeth. When the light is off (Figure 3-7a), the PLCN gear remains inactive and preserves its initial conformation

[2] Completed in collaboration with Bioinspired Materials Lab at the University of Michigan

(i.e., flat, non-deformed), locking with the gear train and receiving power (engaged). When the light is on (Figure 3-7b), the illuminated PLCN gear teeth bend downwards (submerged) to interrupt the power transmission (while the driving and idle gears are moving, the clutch gear does not). If the light stimulus is not applied directly to the desired teeth only, accidental flood illumination may occur, which will increase the temperature of the surrounding water. As the surface tension of water decreases with temperature, excess illumination outside of the clutch teeth might slow down (and even "stall") the gear train due to thermocapillary convection competing with the Marangoni propulsion.

PLCNs offer fast gear teeth actuation at low temperatures while producing enough work to break the surface tension of the air–liquid interface and submerge underwater. This actuation of PLCN teeth results in the disengagement of the gear from the mechanical device, effectively acting as a reversible clutch mechanism: power transmission throughout the gear train is interrupted on-demand, while the rest of the components remain free to move.

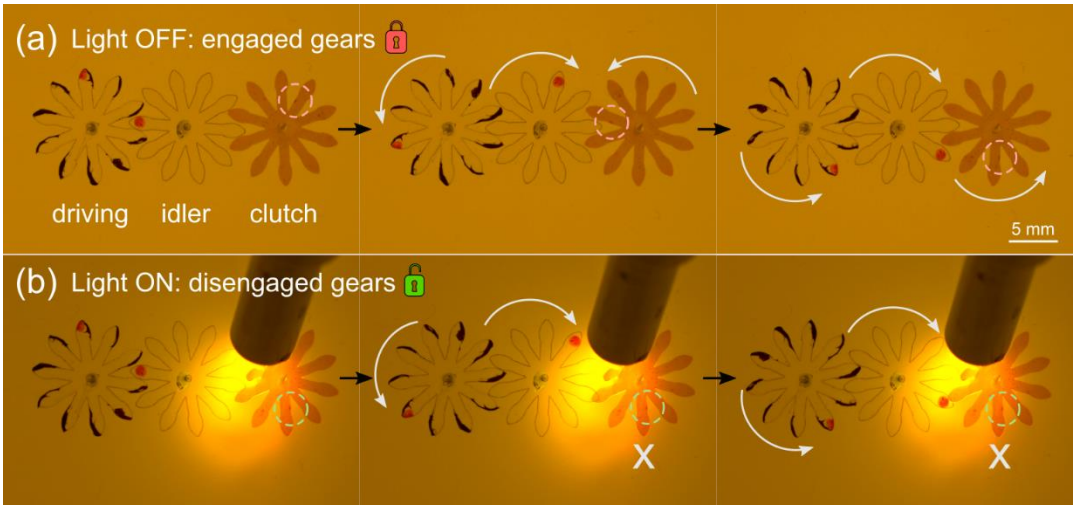


Figure 3-7 Power transmission through a gear train system with active gears (self-propelled driving gear and a liquid crystal network clutch). a) Without light, gears are engaged and power is transmitted throughout the gear train; b) when illuminated, the active PLCN gear deforms and disengages from the gear train, interrupting power transmission (X) and effectively acting as a clutch mechanism.

3.4 Conclusion

A milliscale gear train power transmission is used to showcase the use of protein chemical motors and PLCNs for untethered powering and control, respectively, for small-scale multicomponent mechanical devices. The driving gear containing chemical motors provides power to the system, while the PLCN gear acts as a clutch, disengaging and halting the power transmission through the gear train when illuminated. The driving gear is powered by Marangoni propulsion forces generated by functional motor coatings applied to the driving gear teeth. These motor coatings are composed of a structural protein matrix infused with low surface tension chemical fuel that is released at the air–water interface (thus generating Marangoni flows). These motor protein-fuel complexes can propel a set of gears with high efficiency for prolonged periods of time with a single coating application, effectively acting as the main power source for the mechanical device. In parallel, the clutch gear is composed of plasticized liquid crystal networks with increased energy conversion efficiency and reduced T_g for optimized photothermal bending actuation. The combination of these Marangoni protein motors and photothermal LCNs provides an orthogonal untethered actuation method for selective control of the functions of mechanical devices (in this case, a small-scale power transmission). Such hybrid systems will offer new actuation, powering, and control strategies for multicomponent and multifunctional small-scale devices with potential solutions to the miniaturization challenges of untethered mechanical micromachines.

Chapter 4
Photochemical Liquid Crystal Networks and Chemical Motors

4.1 Introduction

The previous chapter showcased the use of protein motors and LCN's in tandem for the powering and control of a multi-component mechanical device; however the active components were separate from each other. In this work we showcase the integration of protein motors directly onto a photo-active LCN milli-scale swimmer for active, untethered powering and control of a single device. The device and its mechanism of movement is inspired by the Microvelia, a small aquatic bug that harnesses the Marangoni force for propulsion (Figure 4-1a)[156]. The protein motors are applied to an LCN V-shaped swimmer to create propulsion through Marangoni forces. A photochemical LCN is used because it can maintain deformation without continuous light exposure. The swimmer is propelled forward by the motors, and targeted bending of the swimmer's legs is used to control the direction of movement (Figures 4-1b and 4-1c). In addition to straight, forward movement, two different angles of rotation can be achieved through bending the left or right leg downwards into the water. The swimmer can be directed to rotate clockwise or counterclockwise by bending either the right or left leg, respectively.

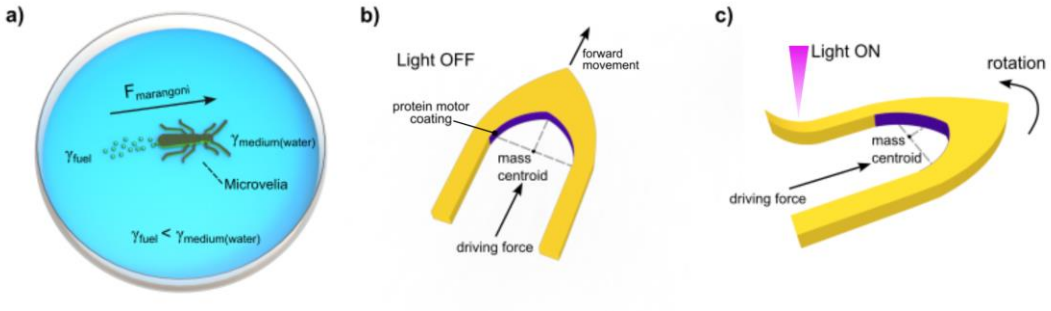


Figure 4-1 a) Microvella mechanism of movement at the air-water interface; b) LCN swimmer movement; c) LCN swimmer movement upon shape change from UV light exposure

4.2 Materials & Methods

4.2.1 Materials

Mono-functional monomer 4-(6-acryloxy-hex-1-yl-oxy)-phenyl 4-(hexyloxy)-benzoate (M1), bi-functional monomer 1,4-bis-[4-(6-acryloyloxyhexyloxy) benzoyloxy]-2-methylbenzene (M2), and photo-active bi-functional azobenzene monomer 4,4'-Bis[9-(acryloyloxy)nonyloxy]azobenzene (M3) were purchased from SYNTHON Chemicals GmbH & Co. KPG.

Bis(2,6-difluoro-3-(1-hydropyrrol-1-yl)phenyl)titanocene (Irgacure 784), polyvinyl alcohol, N,Ndimethylformamide (DMF), 1,1,1,3,3,3-hexafluoro-2-propanol (HFIP), and crystal violet dye were purchased from Sigma-Aldrich. Polyimide SE-5661 was donated by Nissan Chemical Industries.

All reagents and solvents were used as received without further purification. The squid sucker ring teeth (SRT) proteins were extracted from Loligo Vulgaris squid species and purified as described in other work.[171]

4.2.2 Fabrication of LCN-Based Swimmer

The LCN swimmer was fabricated by injecting a mixture of M1, M2, and M3 monomers into capillary cells (50 μm gap) with pre-determined molecular alignment at 115 °C, which is above the mixtures clearing point (T_{NI}). The cell and mixture were then slowly cooled to below T_{NI} to its nematic mesophase, at temperatures ranging from 78°C to 95°C depending on the mixture composition. The mixture was then cross-linked via photo-polymerization using green light, with a wavelength of 565nm. The LCN film was machined to the correct shape using a Universal Laser Systems laser cutter. Further details on the fabrication and molecular alignment of the swimmers can be found in Section 4.3.2.

4.2.3 Materials Characterization

The glass transition and nematic-to-isotropic temperautres (T_g and T_{NI}) of the P50-6 composition were estimated through a phase study using a cross polarized microscope. Polymerization temperatures for the different compositions were determined based on that estimate. The swimmer with applied protein motor coating was analyzed by Fourier Transform Infrared (FTIR) spectroscopy in a ThermoFisher Nicolet iS20 spectrometer with an Attenuated Total Reflection Accessory.

4.2.4 Actuation Characterization

The photochemical actuation behaviour of the swimmer was estimated using splay aligned cantilevers. To determine bending behaviour, one-end fixed cantilevers were exposed to light from a Lumen Dynamics X-Cite XLED source. The tip displacement was determined using a digital microscope (Dino-lite) and measured manually using the Dino-lite software. The elastic modulus was determined through tensile testing using a CellScale Univert tensile machine with a load cell of 10N.

4.2.5 Swimmer Characterization

The LCN swimmer was laser-micromachined from 50um thick LCN films to the desired swimmer design. A protein motor coating consisting of purified SRT protein dissolved in hexafluoroisopropanol (HFIP) at a concentration of 50 mg/mL was applied to the cavity of the swimmer. The coated swimmer was dried in a fume hood prior to testing. Once the coating was dry, the swimmer was exposed to UV light to bend either the left or right leg. A Petri dish was filled with deionized water, and the swimmer was placed at the air-water interface. The performance of the swimmer was recorded with a Nikon D3500 camera, and the swimmer's movement was analyzed using ImageJ software.

4.3 Results & Discussion

4.3.1 Protein Motors for Movement Generation and Swimmer Design[3]

As in the previous section, power is generated through the use of a functional protein motor consisting of HFIP fuel in an SRT protein matrix. The slow release of the low surface tension HFIP fuel from the protein matrix into the water creates a surface tension gradient (Figure 4-2). This gradient generates a propulsive force towards the higher surface tension. When applied to a lightweight polymer construct at the air-water interface, it will cause the construct to move across the surface of the water. More details on the synthesis and fabrication of the protein motor coating can be found in Section 3.2.1.

[3] Completed in collaboration with Bioinspired Materials Lab at the University of Michigan

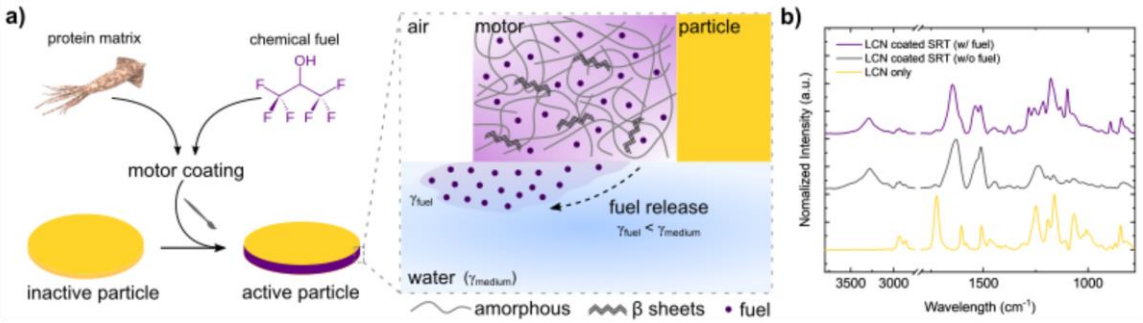


Figure 4-2 a) Application of functional motor coating consisting of chemical fuel entrapped in a protein matrix for an active particle; b) chemical analysis of motors in the LCN swimmer by FTIR.

When the protein motor coating is applied to the entirety of a circular disc, it will result in random (isotropic) movement of the swimmer, as can be seen in Figure 4-3a. However, when the coating is applied to just one side of the same particle, directional (anisotropic) movement can be achieved, as seen in Figure 4-2b. A comparison of the trajectories of swimmers with isotropic versus anisotropic movement can be seen in Figure 4-3c.

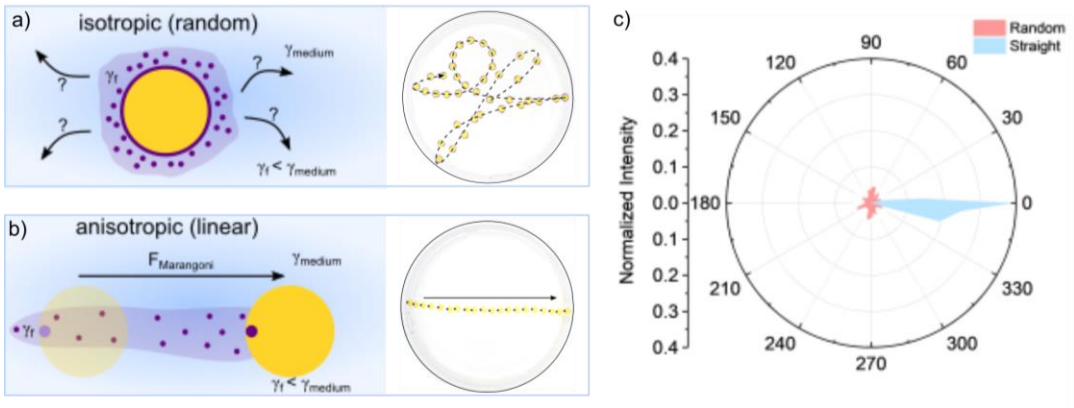


Figure 4-3 The protein motor coating is applied to a particle for a) isotropic and b) anisotropic movement; c) direction of isotropic versus anisotropic movement.

To improve the hydrodynamics, the swimmer was designed and fabricated with a V-shape. The application of the protein motor coating to the cavity of the swimmer results in propulsion, as shown

in Figure 4-4b. The shape of the swimmer also allows for directional control through actuation of the legs. While the swimmer can easily be fabricated at different characteristic lengths (Figure 4-4a), the size of the swimmer will affect its movement on the water, in terms of both direction and speed. It was previously found, using the same protein motor coating, that the speed of the swimmer increases with decreasing characteristic length, whereas the mobility lifetime increases with increasing characteristic length. Additionally, as the characteristic length increases from <1mm to 10mm, the movement of the swimmer changes from solely forward propulsion to partial lateral propulsion.[158] In this work, the use of an active material for steering also needs to be taken into account. The swimmer should have a large enough characteristic length to achieve a useful amount of bending. The aspect ratio of the swimmer's legs was also determined in part based on the bending behaviour of the LCN, which will be discussed further in Section 4.2.3. Based on the movement and bending behaviour of the swimmer, a characteristic size of 10 mm was chosen. As a result, movement when the swimmer is symmetrical (aka flat) is primarily forward but with some lateral movement.

In order to simulate the impact of breaking the symmetry of the swimmer through actuating the legs, the movement of the swimmer with either its left or right leg cut shorter was studied. We found that breaking the symmetry of the swimmer had a significant effect on the direction of movement, while having minimal impact on the speed and duration of movement, as can be seen in Figure 4-4e. Cutting short the left or right leg caused the swimmer to rotate counter-clockwise or clockwise, respectively (Figure 4-4c). While drag forces are smaller on the side with the shorter leg, since there is less of the swimmer in contact with the water, the asymmetry of the swimmer results in asymmetric distribution of the HFIP on the surface. The HFIP will spread towards the side with a shorter leg, resulting in a surface tension gradient that leads to movement at angles up to 60° (Figure 4-4e).

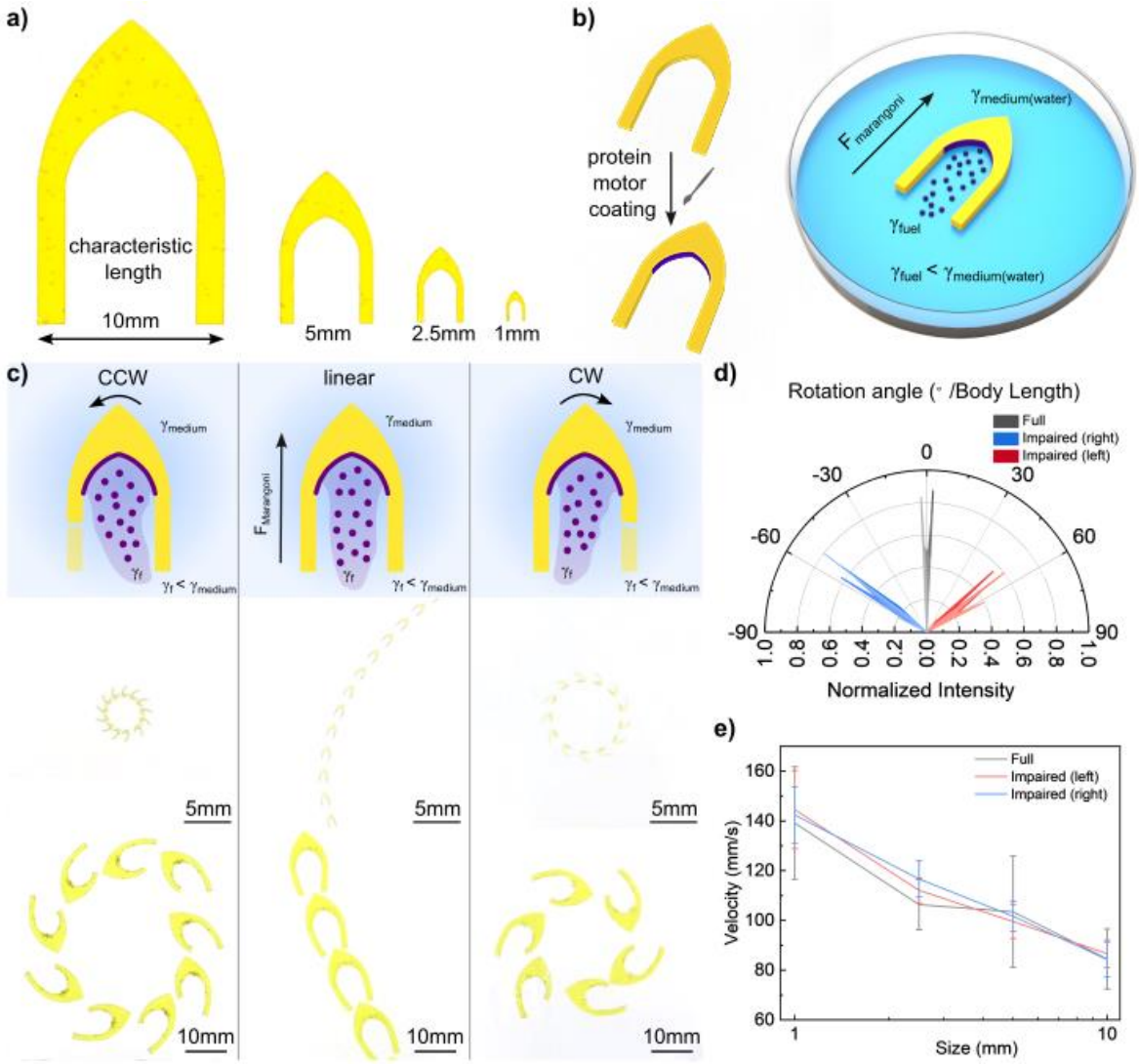


Figure 4-4 a) Characteristic lengths of the in-active V-shaped swimmer; b) protein motor coating is applied to the cavity of the swimmer. This results in forward propulsion of the swimmer at the air-water interface; c) the left and right leg of the swimmer are cut shorter to simulate the effect of asymmetry on swimmer movement. The left leg cut shorter results in counter-clockwise rotation, symmetry results in primarily forward propulsion, and the right leg cut shorter results in clockwise rotation; d) the rotation angle for the three swimmer configurations; e) the velocity of swimmers of different characteristic lengths for each configuration.

4.3.2 Liquid Crystal Network Design

The photo-active swimmer was fabricated out of an acrylate based liquid crystal network containing an azobenzene liquid crystal crosslinker (Figure 4-5a). The LCN is composed of a side-chain mesogenic mono-acrylate backbone (M1: 60 mol%), a mesogenic diacrylate crosslinker (M2: 32 mol%), and a photo-active mesogenic diacrylate azobenzene crosslinker (M3: 8 mol%). The azobenzene compound selected undergoes a *trans*-to-*cis* isomerization upon exposure to UV light, and the reverse *cis*-to-*trans* transition upon exposure to blue or green light. Irgacure 784 (1 wt%) was selected as the photoinitiator, as it can be initiated using visible light, rather than UV. Using green light (565 nm) to initiate polymerization ensures that the azobenzene in the LCN is in the *trans*-state during polymerization.

There are two primary methods used to achieve actuation in azobenzene containing LCNs. The first method uses a planar alignment of liquid crystal moieties and *cis* versus *trans* isomer gradient across the depth of the LCN to achieve bending; in which the surface exposed to UV has a high percentage of *cis*-isomers and the opposite surface has a low percentage resulting in bending towards the light. The other method utilizes a splay alignment of the liquid crystals to achieve bending, with a high conversion of *trans*-to-*cis* across the entire depth of the sample. We chose the second method, utilizing a splay alignment to achieve bending, as we found it resulted in a greater tip displacement upon exposure to the same light intensity as a planar sample. When exposed to UV light, the azobenzene compound will transition from *trans*-to-*cis*, reducing the order of the liquid crystals. As shown in Figure 4-5b, this causes the side with homeotropic alignment of the liquid crystals to expand, while the opposite side with planar alignment will shrink, resulting in bending.

Alignment of the liquid crystals was achieved prior to polymerization using surface anchoring to a glass cell with patterned surfaces. The planar slide was coated with PVA through spin coating, then rubbed unidirectionally with velvet to align the surface. The other glass slide, with homeotropic alignment, was fabricated through spin coating with polyimide followed by a post-bake. The glass cell was constructed with a spacing of 50um and conventional capillary filling was used, as shown in Figure 4-5c. After crosslinking of the LCN using green light, the alignment was confirmed using cross-polarizers. The film was then cut into the desired V-shape for further testing using laser micromachining.

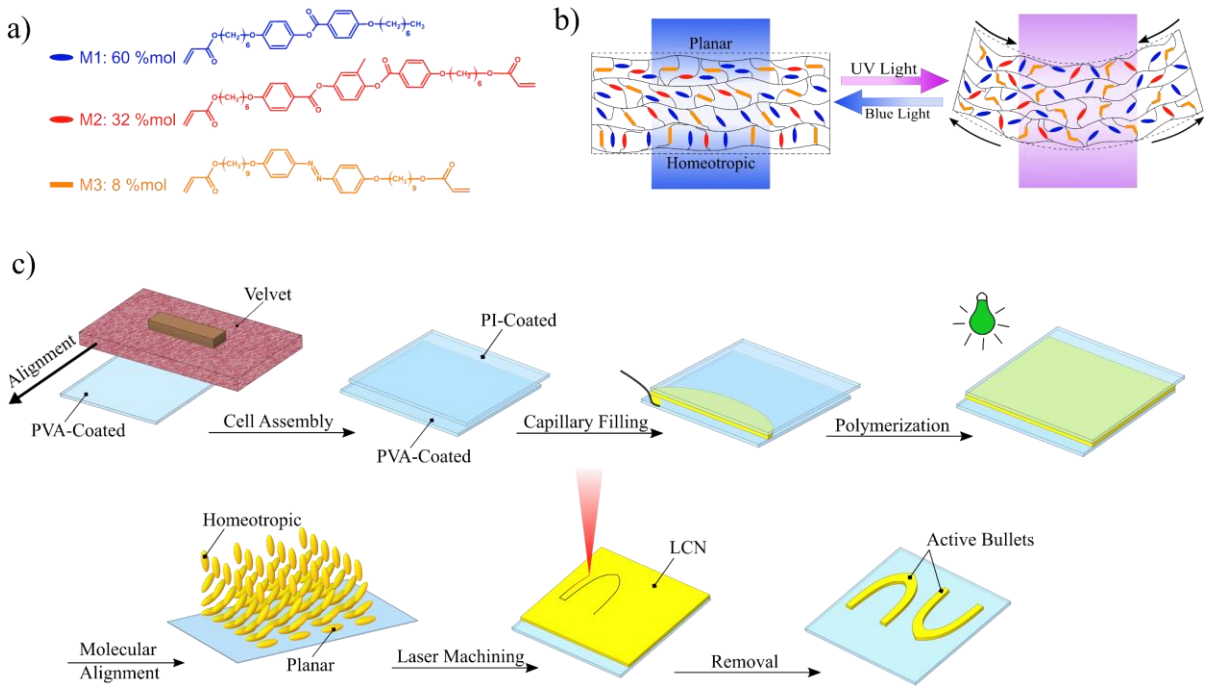


Figure 4-5 a) Molecular structure of constituent molecules in LCN swimmer; b) mechanism of photochemical bending deformation and relaxation in LC-based crosslinked networks; c) Fabrication schematic view of the LCN swimmer fabrication with pre-determined molecular alignment. Molecules have a planar alignment on the side of the cell with the PVA coating. Molecules are aligned homeotropically on the other side of the film, with the polyimide coating.

4.3.3 Liquid Crystal Network Characterization

To achieve optimal swimmer performance, the fabricated LCN network needed to meet three functional requirements. These were 1) change shape quickly on demand, 2) relax quickly on demand, and 3) maintain the shape change without continued external stimuli. The shape change needs to be maintained for a long enough period of time to be useful for directional control of the swimmer. Requirements 1 and 2 are met through the use of a photochemical LCN; the azobenzene moiety selected undergoes a *trans*-to-*cis* isomerization under exposure to UV light and the reverse *cis*-to-*trans* isomerization under exposure to blue light. This causes fast bending and relaxation of the LCN on demand. The azobenzene compound selected also has a *cis*-lifetime that is long enough to result in held shape change when UV light exposure is ceased. While the lifetime of the shape change does not

perfectly match the lifetime of the azobenzene's meta-stable *cis*-state, as other factors also have an effect, the two lifetimes are coupled. The other factors that affect the lifetime of held shape change will be further discussed later in this section. The third requirement is crucial to the operation of the swimmer, and also the most difficult to meet. In addition to the LCN having a sufficient bent lifetime, it also needs to be able to withstand the forces acting upon it when placed on the air-water interface, most notably capillary force which works to flatten the sample. There are a number of different factors that must be considered when optimizing the LCN to meet this requirement.

The ability of water to deform an elastic material is referred to as elastocapillarity. This effect becomes important when the characteristic size of the structure being studied is smaller than the elastocapillary length of the material it is composed of. In order to withstand capillary force long enough for the swimmer to be functional, we want to design the LCN to minimize the elastocapillary length. The elastocapillary length of a material is proportional to the ratio of surface energy to elastic modulus, so there are two different ways to reduce it. The first is to reduce the surface energy of the material, for example through surface treatment, and the second is to increase the elastic modulus of the material through changing its composition. Reducing the surface energy is quite straightforward and was easily achieved through silane treatment. Silanization makes the LCN hydrophobic; its contact angle with water increased from 67.7° pre-treatment to 90.6° post-treatment.

While adjusting the composition of the material can be used to increase elastic modulus, the composition obviously significantly impacts the LCN's shape change behaviour as well. As such a balance must be found between the optimal composition for minimizing elastocapillary length and the optimal composition for maximizing bending. The effect of changing composition on the surface energy of the LCN is assumed to be negligible, as changes in the LCN's contact angle with water were negligible. To determine the best composition for the swimmer five different formulations were tested, with either 6 or 8 mol% azobenzene and total crosslinking mol% ranging from 28 mol% to 65 mol%. The different compositions are named PX-Y, where Y is the mol% of azobenzene and X is the total mol% of crosslinking, including azobenzene. To simulate the actuation behaviour of the legs of the swimmer, rectangular strips of similar aspect ratio were tested. The bending behaviour upon exposure to UV and blue light and the maximum bending achieved for each composition are shown in Figure 4-6a and Figure 4-6b, respectively. All the compositions show on-demand bending, a shape change lifetime of at least 2.5 minutes, and on-demand relaxation. As can be seen in Figure 4-6b, increasing the degree of crosslinking in the sample increases the amount of bending, up to a threshold after which

further increases in degree of crosslinking results in a reduction in bending. This shows that a minimum amount of crosslinking is needed to effectively translate the order-to-disorder transition of the liquid crystals into macroscopic shape change. However, as crosslinking also increases the stiffness of the material, too much crosslinking makes the material more difficult to bend thus reducing the maximum tip displacement achieved. Additionally, it has been shown that strain on azobenzene crosslinkers in a liquid crystal network reduces its *cis*-lifetime. The increase in stiffness is reflected in the elastic modulus of the material, and therefore the elastocapillary length. As shown in Figure 4-6b, the elastocapillary length decreases with increasing crosslinking percentage. Note that elastocapillary length is represented as 1/E, as there is no change in surface energy between the different compositions. Composition P40-8 has the greatest tip displacement of the different compositions.

When comparing samples P38-6 and P40-8, the crosslinking is similar enough to not have a significant impact on the bending behaviour of the material. Therefore, changes in behaviour can be attributed primarily to the increase in azobenzene content. Increasing the azobenzene content from 6 mol% to 8 mol% was found to increase the degree of bending, which can be seen by comparing samples P38-6 and P40-8. However, further increase in azobenzene percent to 10 mol% was found to have a detrimental effect on the ability of the construct to hold its shape change, with partial relaxation occurring immediately upon ceasing light exposure. Based on the bending behaviour of the different samples as well as the elastocapillary lengths, composition P40-8 was selected for fabricating the swimmer. The LCN was designed to withstand elastocapillary forces for a timescale long enough to be useful for directional control of the swimmer. The LCN was not able to overcome the additional forces caused by surface tension to bend while at the air-water interface; instead samples were bent in the air and then placed on the water surface.

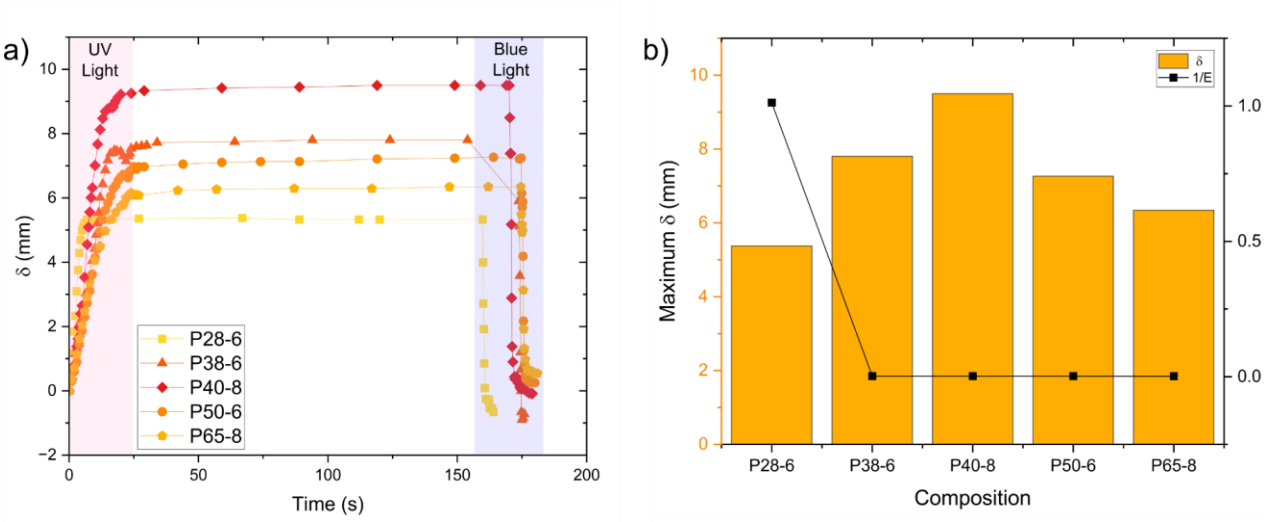


Figure 4-6 a) Bending and relaxation behaviour of different LCN compositions upon exposure to UV and blue light; b) maximum tip displacement and (elastic modulus)$^{-1}$ for tested LCN compositions.

To further study the bending behaviour of the selected LCN composition (P40-8), its response to UV and blue light in air was compared with its response when submerged in water (Figure 4-7). Due to the testing configuration, the tip of the LCN is moving upwards when bending and downwards when relaxing. The slab was able to successfully bend in water, however both the speed of bending and the maximum tip displacement achieved were reduced in water versus air. Water has a significantly higher heat transfer coefficient than air, which results in faster heat dissipation from the LCN construct. While the LCN relies primarily on photochemical effects for deformation, there are still photothermal contributions[145]. When actuating underwater, photothermal effects are greatly reduced or eliminated entirely, resulting in less efficient bending. Additionally, there are also fluid dynamics factors that differ in water versus air. The LCN construct has to overcome a hydrodynamic drag that is two orders of magnitude larger in water than in air (5.0E-05 pa in water vs 2.9E-07 pa in air at maximum bending speed). This significantly slows the speed of bending in water.

The LCN was also found to relax faster in water than air. While in air the LCN relaxation is due to both the photoisomerization of azobenzene from *cis*-to-*trans* and from thermal back relaxation; in water the thermal component is significantly reduced or eliminated. We propose that there are two main reasons for the change in relaxation speed. The first is the hydrostatic pressure on the LCN. At its peak

bent position, the LCN is subject to 273.8 pa of hydrostatic pressure. This pressure is pushing downwards and helps increase the speed with which the LCN straightens out. The second reason for the increased relaxation speed is density changes in the LCN during bending and relaxation. It has been shown that LCNs undergo a significant reduction in density during bending[73]. As such, when the LCN construct is relaxing, it significantly increases in density. This increase in density reduces the construct's buoyancy, which increases the speed with which the construct straightens out.

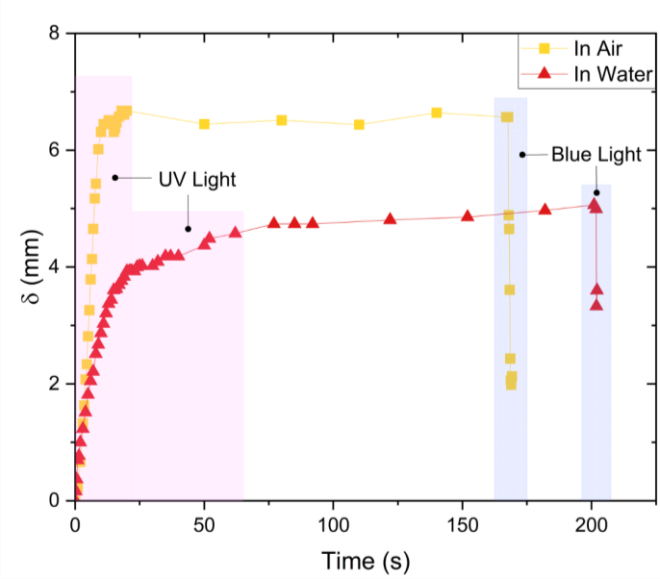


Figure 4-7 Bending behaviour of LCN construct (composition P40-8) in air versus submerged in water upon exposure to UV and blue light.

The final factor examined that influences the amount of bending and behaviour of the swimmer at the air-water interface is the aspect ratio. Samples of different aspect ratios were compared in air and at the surface of water, bending into the water. As shown in Figure 4-8, increasing the aspect ratio results in greater tip displacement. While there is a reduction in the amount of tip displacement when the sample is placed at the air water interface, the trend remains the same. This reduction in tip displacement can be attributed to capillary force acting upon the sample. Based on the bending behaviour an aspect ratio of 10 was selected, with the swimmer having an overall characteristic length of 10mm.

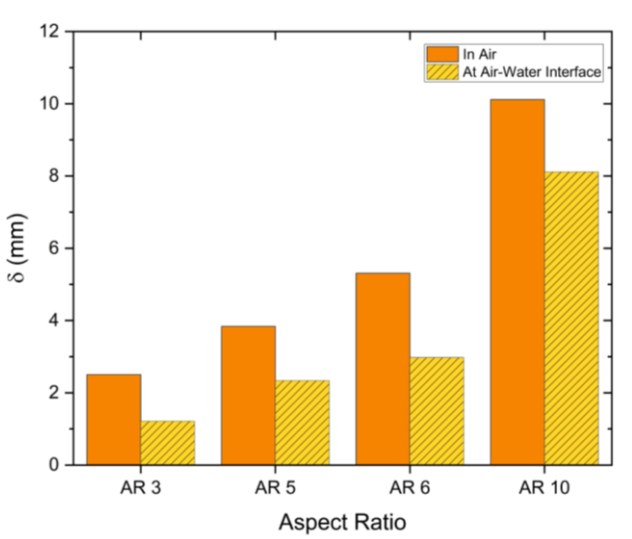


Figure 4-8 Maximum tip displacement of LCN constructs with different aspect ratios in air and when placed at the air-water interface, bent into the water.

4.3.4 Liquid Crystal Network Swimmer Characterization[4]

Once the composition was selected, the LCN swimmer was fabricated and cut out using a laser cutter. The protein motor coating was applied to the swimmer, and successful coating of the protein motors on the LCN was confirmed via FTIR (Figure 4-2b). Prior to application of the protein motor coating, the bending behaviour of the swimmer's legs was confirmed to match the behaviour of the rectangular constructs used for bending characterization. Both the left and right leg showed significant bending upon exposure to UV light (Figure 4-9a) and the ability to withstand elastocapillary force when placed at the air water interface (Figure 4-9b).

Upon application of the protein motor coating, three different modes of movement were achieved through the three different swimmer configurations (Figure 4-9c). With both legs flat on the surface of the water, the swimmer moves forward, with a slight rotation of 0.69° ± 1.31°, as expected based on the testing of the non-photoactive polymer swimmer. When the left leg is bent downwards into the water the swimmer moves counter-clockwise at an average angle of 29.72° ± 9.21°. Similarly, when the right leg is bent downwards into the water, the swimmer moves clockwise at an angle of 34.10° ±

[4] Completed in collaboration with Bioinspired Materials Lab at the University of Michigan

4.83° (Figure 4-9e). The rotation is due to the increase in drag caused by the leg bent into the water. This increase in drag also reduces the speed of the swimmer. The initial velocity of the swimmer in the forward propulsion mode (I) is 68.15 ± 8.18 mm/s. When the left leg (mode II) or right leg (mode III) is bent, the velocity is reduced to 19.25 ±6.11 mm/s and 34.10 ± 4.83 mm/s, respectively. Although the swimmer is symmetrical, there are clear differences in behaviour when the left versus right leg is bent. This may be due to slight differences in the degree of bending or application of the protein motor coating, but further investigation is required to confirm.

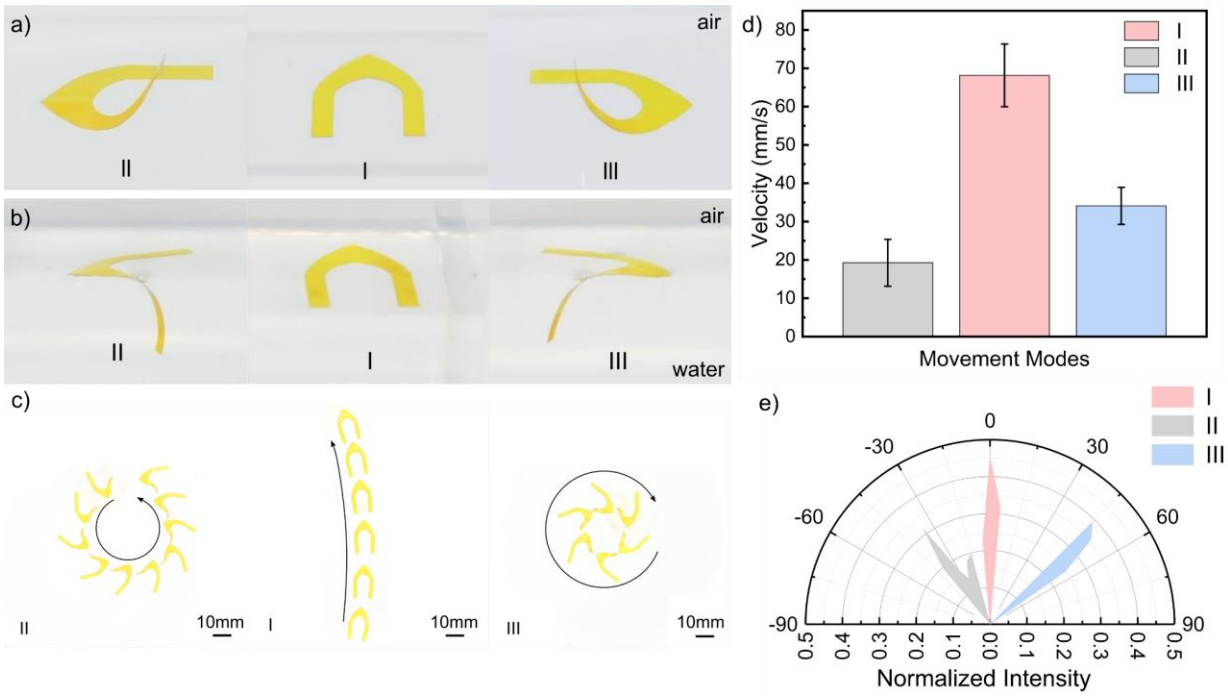


Figure 4-9 a) Three configurations of the active swimmer (left leg bent, flat, and right leg bent) in air; b) three configurations of the swimmer at the air water interface; c) movement of the swimmer at the air water interface for each configuration/movement mode; d) velocity of each movement mode; e) direction of movement for each movement mode.

4.4 Conclusion

Protein motors as a source of untethered powering and LCNs as a method for untethered control were successfully integrated for the fabrication and operation of a milli-scale mechanical device. The swimmer operates at the air-water interface and demonstrates the benefits of decoupling the mechanisms used for powering and robotic function for small-scale soft robotics. The protein motor coating provides the swimmer with propulsion, and the photoactive LCN material is used for directional control. The protein motor coating consists of a low surface tension chemical fuel contained in a structural protein matrix. The fuel is slowly released at the air-water interface, generating a surface tension gradient. This gradient results in Marangoni propulsion towards the higher surface tension. The protein motor coating continuously powers the swimmer with high efficiency and can easily be reapplied once depleted. The swimmer itself is composed of a photochemical LCN film used for directional control. The V-shape of the swimmer allows for the direction of movement to be controlled through targeted shape change. The left or right leg is selectively bent downwards to increase drag forces and results in counter-clockwise or clockwise movement, respectively. The photochemical LCN can be bent on demand, will hold its shape change, and can then be relaxed on demand using UV and blue light for bending and relaxation, respectively. However, bending the swimmer's legs into water results in a significant drop in velocity. Bending the legs upwards, into the air, rather than downwards into the water would resolve this issue and should be explored in future work. Other avenues to explore include varying the degree of bending for greater directional control and relaxing the LCN during swimming to quickly switch from movement modes II or III (primarily lateral movement) to movement mode I (primarily forward movement).

This work showcases not only the benefits of protein motors and LCNs, but also the strong advantage of decoupling locomotion and function in soft robotics. Through decoupling the mechanisms for powering and control, small scale devices can perform more complex functions with greater efficiency. This approach opens up new potential powering and control strategies for multifunctional small-scale devices as it addresses both the miniaturization challenges of traditional robotics and the efficiency challenges of small scale LCN soft robotics.

Chapter 5
LCN Soft Actuators Fueled by Visible Light

5.1 Introduction

Liquid crystal networks are a promising material for biomedical applications of soft robotics. As demonstrated thus far, they are particularly powerful when used in conjunction with protein motors for orthogonal mechanisms of powering and control. However, the reliance on UV light for LCN actuation severely limits their use in relation to people, due to the safety hazards of UV light. There is a need for LCN actuators that operate efficiently in water and can be controlled through visible light rather than UV. While previous works have developed photothermal LCNs that respond to visible and/or NIR light through careful thermal dopant selection, using dopants such as carbon nanotubes[127-129], graphene[130], or gold nanorods, there are few reported photochemical LCNs that are responsive to visible light[176], and the LCN is tested only in air, not water. It has been shown that the light responsivity and *cis*-lifetime of azobenzenes can be tuned through *ortho*-substitution.[137-139,176] A thorough study looked at the effect degree of substitution had on the absorption spectra and *cis*-lifetime of *ortho*-fluoraminoazobenzenes[140]. One of the designed azobenzene compounds was selected for this work and modified to be bi-functional through the addition of acrylate groups, for integration into an LCN. The resulting photochemical LCN is responsive to both UV and visible light with the potential for long shape-change lifetimes.

5.2 Materials & Methods

5.2.1 Materials

Mono-functional monomer 4-(6-acryloxy-hex-1-yl-oxy)-phenyl 4-(hexyloxy)-benzoate (M1) and bi-functional monomer 1,4-bis-[4-(6-acryloyloxyhexyloxy) benzoyloxy]-2-methylbenzene (M2) were purchased from SYNTHON Chemicals GmbH & Co. KG.

Bis(2,6-difluoro-3-(1-hydropyrrol-1-yl)phenyl)titanocene (Irgacure 784) and polyvinyl alcohol (PVA) were purchased from Sigma Aldritch. Polyimide AL60101 was purchased from JSR Corporation. All reagents and solvents were used as received without further purification.

5.2.2 LCN Actuator Fabrication

A mixture of M1, M2, and M3 was melted at 112°C, which is above the mixtures clearing point (T_{NI}). The mixture was injected into capillary cells with a 20 µm gap and pre-determined molecular alignment. The cell was transferred to a polymerization stage and heated at a rate of 20/min from room temperature (~23°C) to 95°C, where it was held for 4 minutes. The mixture was cooled at a rate of 3°C/min to 75°C, which is above the mixtures T_{NI}. The cooling rate was then reduced to 1°C/min until 57°C, and then further reduced to 0.5°C/min until the polymerization temperature of 52°C was reached. The mixture was crosslinked by photo-polymerization using green light (550 nm), which was used instead of UV to ensure the azobenzene was in the *trans*-state during polymerization. The LCN actuators were cut out by hand using a razor blade.

5.2.3 Materials Characterization

The transition temperatures (T_{NI} and T_g) of the LCN were estimated through a phase study done using a polarized optical microscope. A mixture containing M1, M2, and M3 but no photoinitiator was used to ensure no polymerization occurred during the phase study. The mixture was heated at a rate of 5°C/min to 95°C, then cooled at a rate of 4°C/min to 60°C and 2°C/min to 25°C. The absorption spectra of the azobenzene monomer and LCN film were measured using an Agilent Technologies Cary 60 UV-Vis spectrometer. The azobenzene crosslinker was prepared for measurement in the dark. It was illuminated with 405 nm light for 12 seconds prior to measurement and 595 nm light for 12 minutes prior to measurement. UV-Vis measurements of the LCN film were taken with the film immersed in water and the sample was prepared in the dark. It was illuminated with 405 nm light for 12 seconds prior to measurement and 580 nm light for 12 minutes prior to measurement.

5.2.4 Actuation Characterization

The actuation behaviour of the LCN was measured using an LCN cantilever with a planar alignment. One-end fixed cantilevers were exposed to light from a CoolLED pE-4000 LED light source. The bending behaviour was filmed using a Canon EOS R6 camera (29.97 fps) and measured manually using the Fiji image-processing package.

5.3 Results & Discussion

5.3.1 Novel Azobenzene[5]

The addition of *ortho*-amination to an azobenzene compound works to increase the visible light absorptivity of the compound, while *ortho*-fluorination increases the *cis*-isomer stability. A range of different azobenzene compounds with different degrees of *ortho*-fluoro substitution and either pyrrolidine or piperidine *ortho*-substitution were synthesized and characterized in a previous study.[140] Based on the photochemical properties and thermal *cis*-to-*trans* isomerization lifetime, one azobenzene compound was selected for use. The compound has a single *ortho*-fluoro substitution and a piperidine *ortho*-substitution (Figure 5-1a). The compound isomerizes from *trans*-to-*cis* upon exposure to violet light, from *cis*-to-*trans* upon exposure to green/yellow light, and has a *cis*-lifetime in solution of 72 hours.[140] The structure of the azobenzene compound was modified to add carbon chains ending in an acrylate group in order to make the compound a bi-functional crosslinker (Figure 5-1b). This enables the polymerization of the azobenzene into a liquid crystal network. The absorption spectra of the azobenzene monomer (Figure 4-1c) and the LCN containing the azobenzene (Figure 4-1e) show that the *trans*-isomer has absorption peaks in both the UV and visible light range. In comparison, the absorption spectrum for the azobenzene compound used in the previous section shows the *trans*-isomer has peaks solely in the UV region (Figure 5-1d).

[5] Synthesized by collaborators, Smart Photonic Materials research group at Tampere University

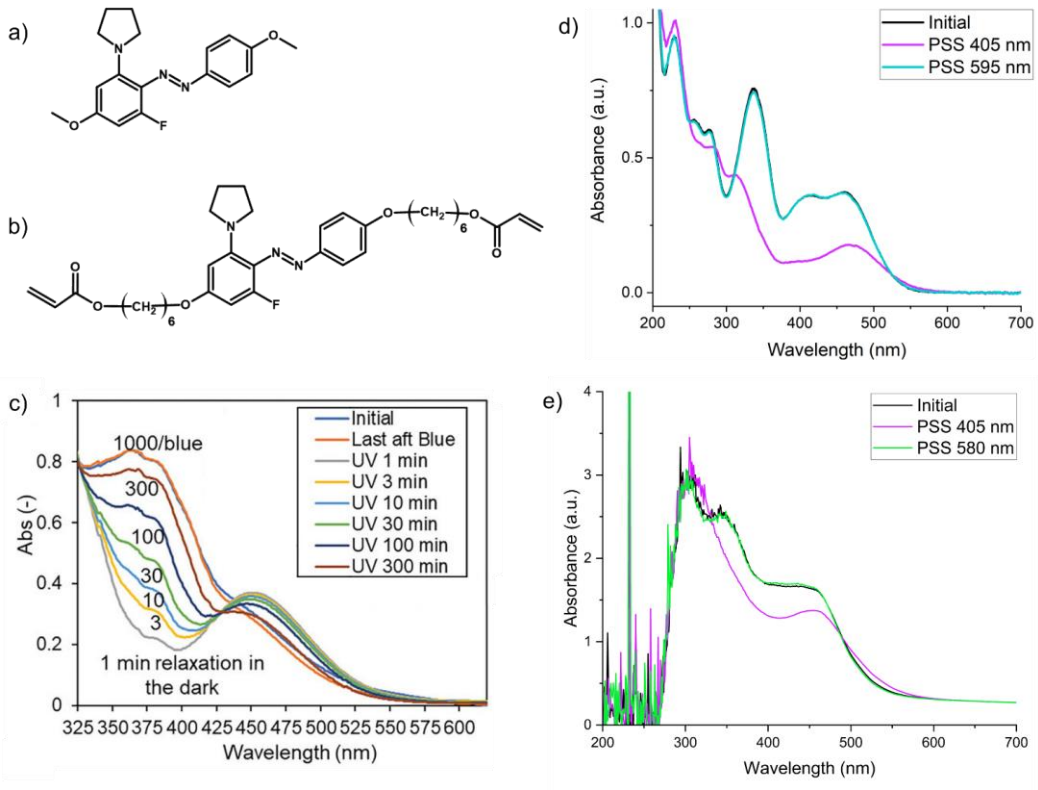


Figure 5-1 a) Molecular structure of the azobenzene photoswitch; b) molecular structure of the azobenzene photoswitch crosslinker; c) absorption spectra for azobenzene DA9AB after UV and blue light illumination. Reproduced with permission.[177] 2021, Wiley; d) absorption spectrum for the novel azobenzene crosslinker after 405 nm and 595 nm illumination; e) absorption spectrum of the LCN containing the azobenzene crosslinker after 405 nm and 580 nm illumination

5.3.2 LCN Actuator Fabrication

The novel azobenzene compound was incorporated into an acrylate based liquid crystal network. The LCN consists of a side-chain mesogenic mono-acrylate backbone (M1: 70 mol%), a mesogenic diacrylate crosslinker (M2: 25 mol%) and the novel photo-active mesogenic diacrylate azobenzene crosslinker (M3: 6 mol%). Irgacure 784 (1wt%) was used as the photoinitiator, and polymerization was initiated using green (550 nm) light; this ensures that the azobenzene is in the *trans*-state during polymerization.

The LCN was fabricated with a planar alignment, wherein bending is achieved through the introduction of a *cis*- to *trans*-isomer gradient across the depth of the sample via exposure to violet light. The surface of the LCN exposed to the light has a high percentage of *cis*-isomers that leads to compression whereas the opposite surface has a high percentage of *trans*-isomers with no compression or expansion. This results in the LCN bending towards the light source (Figure 5-2a). Continued light exposure will then result in the LCN flattening out as the azobenzene is fully isomerized to the *cis*-isomer. As with the photochemical LCN studied in the previous section, a splay alignment was found to lead to greater bending than planar, however it also was found to significantly reduce the lifetime of the shape change. With a splay alignment, the LCN would relax immediately upon ceasing light exposure, whereas with a planar alignment the LCN would better hold the shape change until exposed to green/yellow light.

Alignment of the liquid crystals was achieved prior to polymerization using surface anchoring to a glass cell with patterned surfaces. Both sides of the cell were coated with PVA through spin coating, then rubbed unidirectionally with velvet to align the surface. The glass cell was constructed with a spacing of 20um and conventional capillary filling was used, as shown in Figure 5-2b. After crosslinking of the LCN using green light, the alignment was confirmed using cross-polarizers. The film was then cut into the desired shape for actuation characterization.

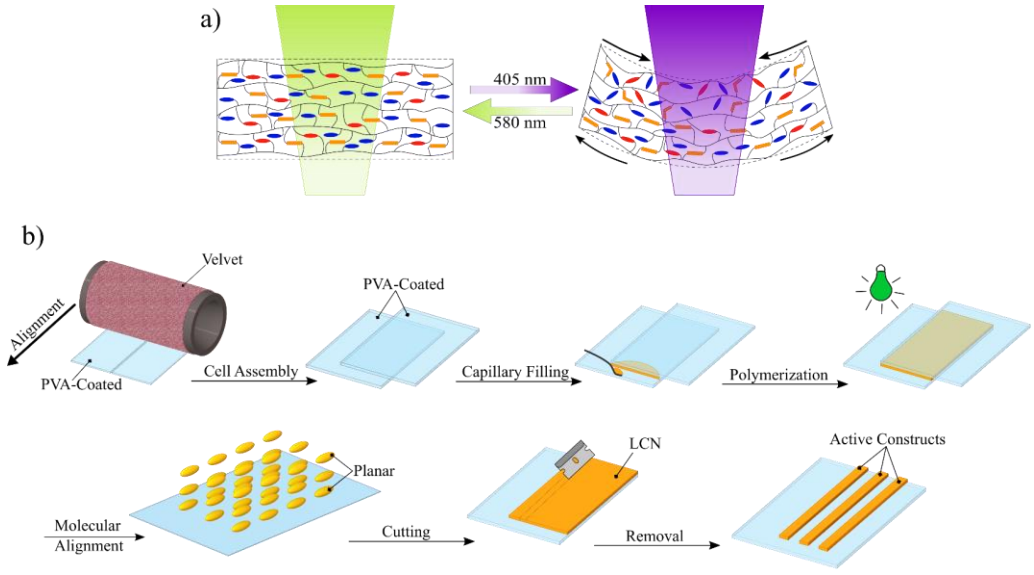


Figure 5-2 a) Mechanism of bending and relaxation in the photochemical LC-network; b) fabrication procedure for the LCN.

The structure of the mesogens used can be seen below in Figure 5-3a. The azobenzene crosslinker has a pyrrolidine *ortho*-substitution, which serves the purpose of increasing the *cis*-lifetime of the compound. However, it also increases the size of the molecule and will significantly increase the free volume in the LCN. The *ortho*-substitution on the azobenzene crosslinker also had a significant effect on the alignment of the liquid crystals. Surface anchoring is a commonly used method for LC alignment and was successfully used in the previous section for a similar LCN, however complete alignment of this LCN couldn't be achieved. The alignment was found to vary across the cell, with samples containing 2 or 3 regions of different levels of alignment (Figures 4-3d, 4-3e, and 4-3f).

We theorize that the variation in alignment within the cell is due to shear force improving the alignment of the liquid crystals. The location of the well aligned versus poorly aligned segments was consistent across all samples fabricated. The well aligned segment is always at the opposite end of the cell from where the melted mixture was introduced. It is proposed, therefore, that the shear force acting on the mixture during capillary filling is responsible for helping align the liquid crystals, with the sections that experienced the greatest shear force (i.e. travelled furthest through the cell) having better alignment. The surface of the glass slides (z-direction) and edges of the cell (x-direction) impose no-slip boundary conditions on the fluid. Under no-slip boundary conditions, the liquid experiences the

highest shear stress at the boundaries and no shear stress at the very centre of the cell. The effect of shear on alignment can be seen in the shape of the transition between the poorly aligned and well aligned sections. As shown in Figure 5-3b the boundary between the two regions is curved and matches the inverse of the shear stress profile,[178] i.e. the edges experience the highest amount of shear stress and are therefore aligned earlier than the centre. It was found that increasing the thickness of the cell from 20µm to 50µm reduced the size of the well aligned area. Increasing the aspect ratio of the cell, which reduces the characteristic length scale in the x-direction, was found to increase the size of the aligned area. This further supports the theory that shear stress contributes to alignment, as shear rate scales inversely proportional to length scale for microfluidics.[179] While reducing the azobenzene crosslinker content improved alignment, it significantly reduced the bending performance, so was kept at 6 mol%.

A phase study was done using a polarized optical microscope to determine the effect of polymerization temperature on the alignment, and to estimate the optimal polymerization temperature. The phase study was done on a cell with a 20um gap, and photoinitiator was excluded from the mixture to avoid any polymerization. Figure 5-3b shows the POM images 30, 50, and 60°C, where the upper left section is well aligned, and the lower right section is poorly aligned. It was found that the well aligned and poorly aligned sections of the cell would undergo phase transitions at different temperatures. Both sections had a T_{NI} of approximately 70°C, however the poorly aligned section had a T_g of approximately 50°C whereas the aligned section didn't show a glass transition even when cooled to below 0°C. We theorize that the solution undergoes supercooling, as it would crystallize when left at room temperature (~23°C) for at least 12 hours. Due to this, the polymerization temperature of 52°C was selected based on the T_g of the poorly aligned section.

The rate of cooling also has an impact on the LCN alignment. Cooling at a rate of 1°C/min resulted in samples with two different regions of alignment. The first region (Figure 5-3d) had poor alignment and no shape change behaviour. The second region (Figure 5-3e) had improved alignment and demonstrated reversible shape change behaviour. However, the entire sample had a significant number of disclination line defects, which are discontinuities in the programmed director field of the LCN.[180] The disclination lines can be clearly seen to have different alignment to the rest of the LCN in Figure 5-3e. Reducing the cooling rate to 0.5°C/min resulted in a third region of alignment in the LCN. The region is located at the end of the cell and is therefore the section that has experienced the highest shear

force. This region has the best alignment, with no disclination lines, however it still has a number of point defects as can be seen in Figure 5-3f.

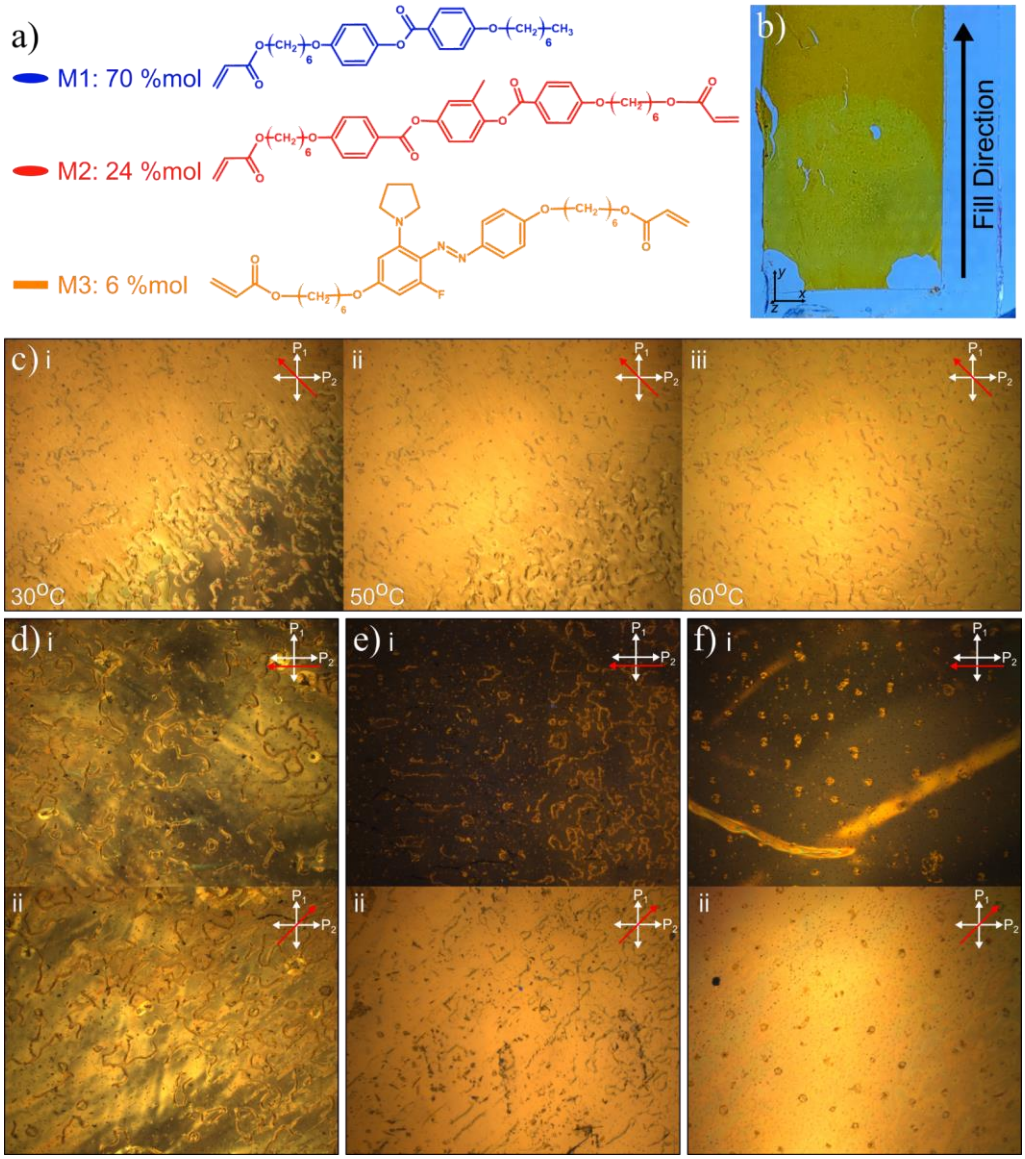


Figure 5-3 a) Molecular structure of the monomer constituents of the LCN; b) LCN in a glass cell showing change in alignment across the length of the cell; c) POM images of the phase study of the LCN; d) POM images of the poorly aligned section of the LCN; e) POM images of the well aligned section of the LCN with disclination line defects; f) POM images of the well aligned section of the LCN with point defects.

5.3.3 LCN Actuator Characterization

The novel azobenzene crosslinker used in this work was designed to have absorption peaks in the visible light range to achieve LCN shape change behaviour in response to visible light. The absorption spectra in Figure 5-1d and 5-1e show that the monomer and LCN have absorption peaks in both the UV and visible light range. The bending behaviour of the LCN in response to wavelengths ranging from 365 nm to 460 nm was studied. The bending and relaxation behaviour using different wavelengths for bending and 550 nm light for relaxation is shown below in Figure 5-4. In all cases, the LCN bends quickly in response to light, reaches a maximum tip displacement and then begins unbending. It is important to note that this isn't due *cis*-to-*trans* isomerization of the azobenzene, but rather the planar alignment of the samples. Since the bending is caused by a gradient of *cis*- to *trans*-isomers, continued light exposure once maximum tip displacement has been reached will result in a loss of the gradient as the azobenzene throughout the entire depth of the sample isomerizes from *trans*-to-*cis*.

As expected, based on the relative intensities of the absorption peaks, the LCN has greater tip displacement in response to UV light (365 nm & 385 nm) than visible light (405 nm, 435 nm, and 460 nm). While the amount of bending is lower in response to the visible wavelengths, there is still enough bending to be useful for potential applications. The reduction in bending is outweighed by the gained benefits of improved safety for use in biomedical applications through the use of visible rather than UV light.

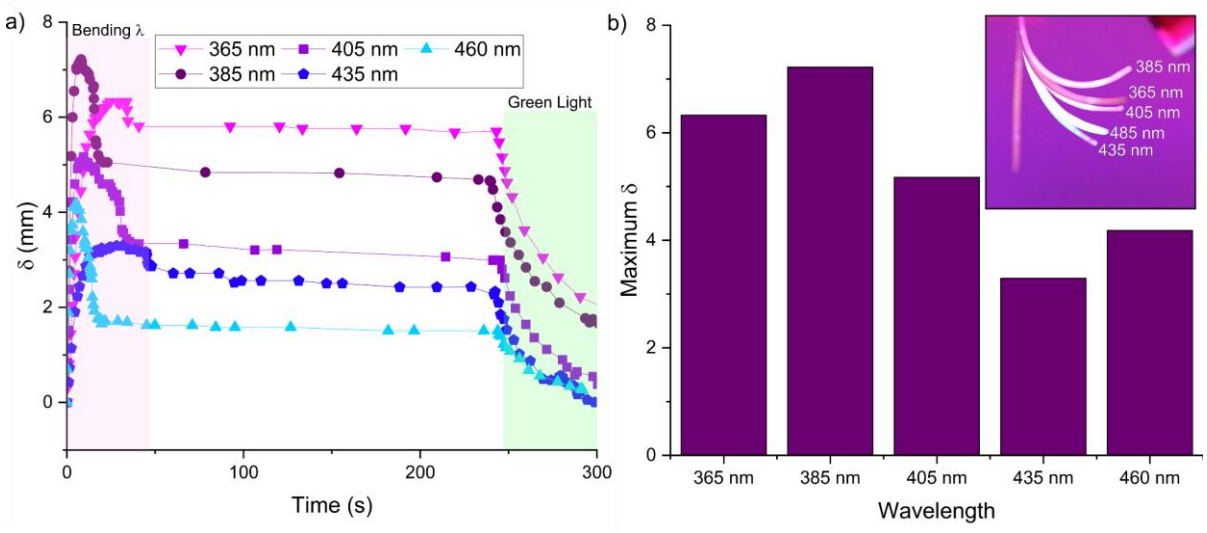


Figure 5-4 a) Bending and relaxation of the LCN over time upon exposure to different wavelengths for bending; b) maximum tip displacement of the LCN upon exposure to different wavelengths.

As potential biomedical applications will require the efficient operation of the LCN in flooded media, its bending behaviour submerged in water was also studied (Figure 5-5). As with the photochemical LCN studied in the previous section, there is a reduction in both the speed and magnitude of bending when the LCN is submerged. While the previous (UV-responsive) LCN showed a 24% drop in maximum tip displacement when submerged, this LCN had a 46% drop in maximum tip displacement when submerged. The reduced tip displacement is primarily due to the increased hydrodynamic and hydrostatic forces acting upon the actuator while it is trying to bend. Additionally, any photothermal effects are reduced or entirely eliminated due to the faster heat dissipation in water. The larger drop in degree of bending for the LCN can be attributed in part to the lower mechanical strength of the actuator. At 20μm, it is less than half the thickness of the previous actuator. Increasing the thickness would likely improve mechanical strength, however it reduces the quality of liquid crystal alignment. The slower relaxation can also be attributed to increase hydrodynamic force, as well as a reduction in thermal relaxation.

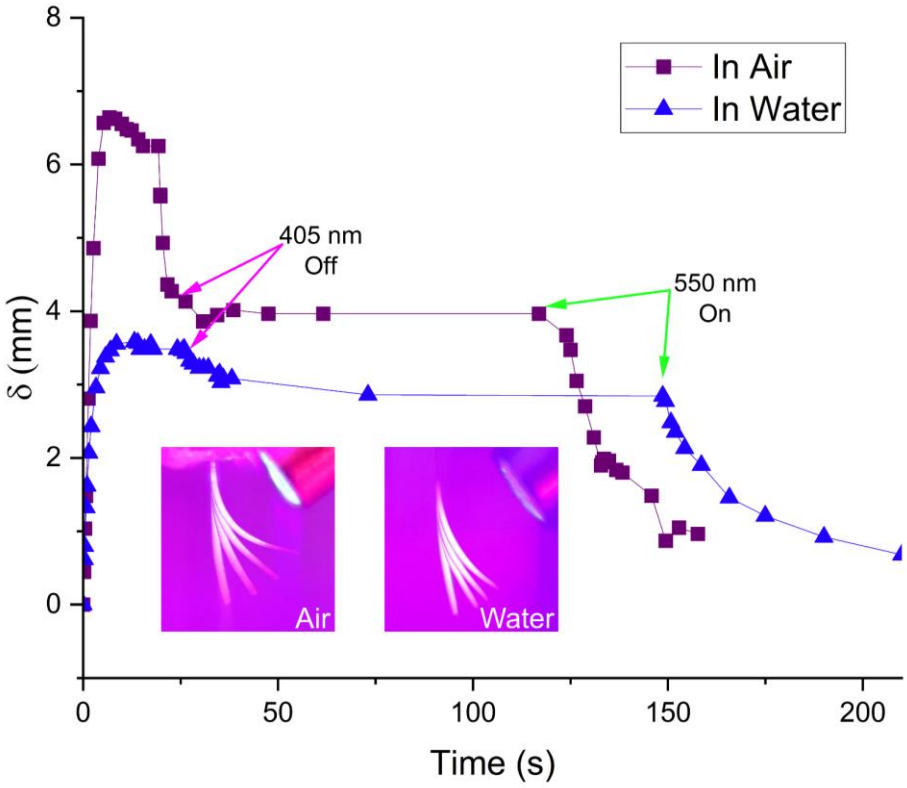


Figure 5-5 Bending behaviour of the LCN upon exposure to violet and green/yellow light in air versus water

As the azobenzene crosslinker was designed to have an extended *cis*-lifetime, the LCN actuators shape change lifetime was examined over a period of ~6 hours (Figure 5-6a). The actuator showed immediate partial relaxation upon ceasing light exposure, followed by a slower reduction in tip displacement over the course of the remaining 6 hours. Further photochemical studies should be done to determine if the relaxation is due to *cis*-to-*trans* isomerization, or other mechanical effects such as stress relaxation. A reduction in lifetime is expected once the azobenzene is incorporated into a network, as has been previously reported.[181,182] This is due to restrictions on molecular movement and steric strain imposed by the network.[181,183] To determine the reusability of the actuator, it was cycled through bending and relaxation 30 times (Figure 5-6b). After the first bending cycle, the actuator did not relax back to the initial position and showed continued drift over the remaining cycles. However, the magnitude of bending remains consistent across the cycles.

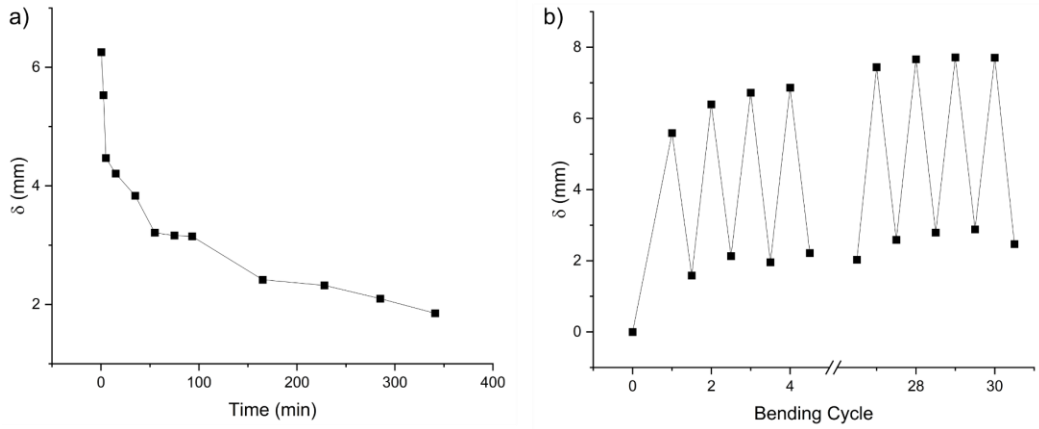


Figure 5-6 a) Lifetime of deformation of the LCN upon initial exposure to 405 nm light; b) performance of the LCN over 30 bending and relaxation cycles.

5.4 Conclusion

A novel azobenzene crosslinking mesogen, designed for visible light responsivity, was successfully integrated into a photochemical LCN. The *ortho*-fluoroaminoazobenzene crosslinker undergoes *trans*-to-*cis* isomerization upon irradiation with violet light, and the reverse *cis*-to-*trans* isomerization under irradiation with green/yellow light. The LCN can be actuated efficiently solely with visible light rather than UV light, an important step towards the use of LCNs in biomedical applications. Efficient functioning in flooded media is another important requirement for biomedical soft robotics, and so the performance of the LCN when submerged was studied. The LCN was successfully actuated in both air and water, albeit with a reduction in bending performance, both in speed and maximum tip displacement, when submerged in water. While the novel azobenzene crosslinker was found to have a lifetime of 72 hours in solution, the lifetime of held shape change by the LCN was significantly shorter. This may be attributed to strain on the azobenzene from the network. The LCN was tested over 30 bending and relaxing cycles, and displayed some drift in the relaxed shape, i.e. it was not able to fully return to the initial position. However, bending magnitude was consistent across the cycles, which demonstrates good longevity of the LCN. The novel visible light responsive photochemical LCN developed in this work is an important step towards the safe use of LCNs for biomedical applications and opens up exciting new research directions in the field.

Chapter 6
Summary and Outlook

Decoupling the powering and control mechanisms for soft robotics is a strong approach for more efficient aquatic soft robotics. This work demonstrated the use of protein motors in conjunction with photothermal and photochemical LCNs for small scale aquatic devices. There are a number of possible research directions to take based upon the work done here. In both case studies the LCN actuators were bent downwards into water due to an inability to withstand or overcome capillary force when bent upwards into the air. Improving the mechanical strength and actuation efficiency to enable actuation into the air while at the air-water interface will improve the versatility of LCN devices and open up new potential applications. The use of visible light rather than UV is also an important area of development. The successful fabrication of a visible light response LCN was discussed in Chapter 5; future work could include improvement of the material and utilization for robotic applications. In particular, the effect of shear on the alignment of the liquid crystals should be further explored. If the monomer mixture is found to display shear thinning behaviour it could potentially be optimized for use in extrusion additive manufacturing.

In this work, decoupling was done through the use of protein motors for powering and LCNs for active control of robotic function. Another promising approach is the addition of magneto-responsivity. Doping LCNs with magnetic microparticles has been reported as an effective way to imbue LCNs with magnetic programming and actuation. This method allows for decoupled locomotion and control of robotic function or bimodal actuation. However, there are still limitations to this approach. A high loading of microparticles is required for magneto-responsivity, which interferes with the liquid crystal alignment and reduces the LCNs performance. As such, there is a trade-off between the magneto-responsivity and photo-responsivity. We propose that the use of ferromagnetic nanoparticles would resolve this dilemma. Specifically, the use of non-toxic iron platinum ferromagnetic nanoparticles, which have successfully been used in micro-robotics but not yet in conjunction with LCNs. We have completed preliminary work on this approach, synthesizing the ferromagnetic nanoparticles (Figure A-1) and conducting initial LCN integration tests. The nanoparticles synthesized had an average diameter of 9.4 nm, and initial use of them as dopants in the photothermal LCN used in Chapter 3 found they had no detrimental effect on liquid crystal alignment and LCN performance. The LCN also displayed good magneto-responsiveness when tested in air and on the surface of water. However, the nanoparticle

doped LCN had a very short lifetime, with the nanoparticles aggregating within the network resulting in a reduction in magnetic responsiveness. Future research should focus on resolving this issue and fully characterizing the photo- and magneto-responsiveness of the material, including different alignment patterning of the magnetic nanoparticles. Additionally, protein motors could be added to achieve untethered powering and bimodal actuation. Further work focusing on the decoupling of locomotion and robotic function will enable more complex soft robotic functions and open up greater possibilities for aquatic soft robotic applications.

References

[1] H. Wang, M. Totaro, L. Beccai, *Adv. Sci.* **2018**, *5*, 1800541.

[2] C. Majidi, *Soft Robot.* **2014**, *1*, 5.

[3] G. M. Whitesides, *Angew. Chem. Int. Ed.* **2018**, *57*, 4258.

[4] J. Fang, Y. Zhuang, K. Liu, Z. Chen, Z. Liu, T. Kong, J. Xu, C. Qi, *Adv. Sci.* **2022**, *9*, 2104347.

[5] C. Laschi, M. Cianchetti, B. Mazzolai, L. Margheri, M. Follador, P. Dario, *Adv. Robot.* **2012**, *26*, 709.

[6] D. Rus, M. T. Tolley, *Nature* **2015**, *521*, 467.

[7] M. Cianchetti, C. Laschi, A. Menciassi, P. Dario, *Nat. Rev. Mater.* **2018**, *3*, 143.

[8] S. I. Rich, R. J. Wood, C. Majidi, *Nat. Electron.* **2018**, *1*, 102.

[9] C. Laschi, B. Mazzolai, M. Cianchetti, *Sci. Robot.* **2016**, *1*, eaah3690.

[10] J. Jiang, Z. Yang, A. Ferreira, L. Zhang, *Adv. Intell. Syst.* **2022**, *4*, 2100279.

[11] S. Chowdhury, W. Jing, D. J. Cappelleri, *J. Micro-Bio Robot.* **2015**, *10*, 1.

[12] M. Li, A. Pal, A. Aghakhani, A. Pena-Francesch, M. Sitti, *Nat. Rev. Mater.* **2022**, *7*, 235.

[13] L. Hines, K. Petersen, G. Z. Lum, M. Sitti, *Adv. Mater.* **2017**, *29*, 1603483.

[14] C. Huang, J. A. Lv, X. Tian, Y. Wang, Y. Yu, J. Liu, *Sci. Rep.* **2015**, *5*, 17414.

[15] M. P. da Cunha, H. S. Kandail, J. M. J. den Toonder, A. P. H. J. Schenning, *Proc. Natl. Acad. Sci. U. S. A.* **2020**, *117*, 17571.

[16] X. Chen, B. Jang, D. Ahmed, C. Hu, C. De Marco, M. Hoop, F. Mushtaq, B. J. Nelson, S. Pané, *Adv. Mater.* **2018**, *30*, 1705061.

[17] J. M. Mccracken, B. R. Donovan, T. J. White, *Adv. Mater.* **2020**, *32*, 1906564.

[18] M. A. McEvoy, N. Correll, *Science.* **2015**, *347*, 1261689.

[19] G. Scalet, *Actuators* **2020**, *9*, 10.

[20] A. Lendlein, *Sci. Robot.* **2018**, *3*, eaat9090.

[21] D. Schönfeld, D. Chalissery, F. Wenz, M. Specht, C. Eberl, T. Pretsch, *Molecules* **2021**, *26*, 522.

[22] Y. Zhang, T. Liu, X. Lan, Y. Liu, J. Leng, L. Liu, *Compos. Commun.* **2022**, *36*, 101383.

[23] E. S. Keneth, R. Lieberman, M. Rednor, G. Scalet, F. Auricchio, S. Magdassi, *Polymers.* **2020**, *12*, 710.

[24] Y. Yang, F. Ma, Z. Li, J. Qiao, Y. Wei, Y. Ji, *J. Mater. Chem. A* **2017**, *5*, 7285.

[25] T. Fang, L. Cao, S. Chen, J. Fang, J. Zhou, L. Fang, C. Lu, Z. Xu, *Mater. Des.* **2018**, *144*, 129.

[26] X. Wang, J. Lan, P. Wu, J. Zhang, *Polymer.* **2021**, *212*, 123174.

[27] X. Huang, M. Ford, Z. J. Patterson, M. Zarepoor, C. Pan, C. Majidi, *J. Mater. Chem. B* **2020**, *8*, 4539.

[28] Y. Xia, Y. He, F. Zhang, Y. Liu, J. Leng, *Adv. Mater.* **2021**, *33*, 2000713.

[29] H. Wang, Z. Zhu, H. Jin, R. Wei, L. Bi, W. Zhang, *J. Alloys Compd.* **2022**, *922*, 166219.

[30] M. Khoo, C. Liu, *Sensors Actuators, A Phys.* **2001**, *89*, 259.

[31] E. Diller, M. Sitti, *Adv. Funct. Mater.* **2014**, *24*, 4397.

[32] J. Kim, S. E. Chung, S. Choi, H. Lee, J. Kim, S. Kwon, *Nat. Mater.* **2011**, *10*, 747.

[33] E. Diller, J. Zhuang, G. Zhan Lum, M. R. Edwards, M. Sitti, *Appl. Phys. Lett.* **2014**, *104*, 174101.

[34] J. Giltinan, V. Sridhar, U. Bozuyuk, D. Sheehan, M. Sitti, *Adv. Intell. Syst.* **2021**, *3*, 2000204.

[35] Z. Ye, S. Régnier, M. Sitti, *IEEE Trans. Robot.* **2014**, *30*, 3.

[36] H. Chung, A. M. Parsons, L. Zheng, *Adv. Intell. Syst.* **2021**, *3*, 2000186.

[37] K. M. Herbert, H. E. Fowler, J. M. McCracken, K. R. Schlafmann, J. A. Koch, T. J. White, *Nat. Rev. Mater.* **2022**, *7*, 23.

[38] O. Erol, A. Pantula, W. Liu, D. H. Gracias, *Adv. Mater. Technol.* **2019**, *4*, 1900043.

[39] I. Dierking, A. M. F. Neto, *Crystals* **2020**, *10*, 604.

[40] K. Sano, Y. Ishida, T. Aida, *Angew. Chem. Int. Ed.* **2018**, *57*, 2532.

[41] X. Du, J. Zhou, J. Shi, B. Xu, *Chem. Rev.* **2015**, *115*, 13165.

[42] Y. S. Zhang, A. Khademhosseini, *Science.* **2017**, *356*, eaaf3627.

[43] A. S. Hoffman, *Adv. Drug Deliv. Rev.* **2012**, *64*, 18.

[44] H. Lee, H. Choi, M. Lee, S. Park, *Biomed. Microdevices* **2018**, *20*, 103.

[45] N. A. Peppas, J. Z. Hilt, A. Khademhosseini, R. Langer, *Adv. Mater.* **2006**, *18*, 1345.

[46] B. V. Slaughter, S. S. Khurshid, O. Z. Fisher, A. Khademhosseini, N. A. Peppas, *Adv. Mater.* **2009**, *21*, 3307.

[47] D. in Kim, H. Lee, S. hyun Kwon, H. Choi, S. Park, *Sensors Actuators, B Chem.* **2019**, *289*, 65.

[48] S. Fusco, H. W. Huang, K. E. Peyer, C. Peters, M. Häberli, A. Ulbers, A. Spyrogianni, E. Pellicer, J. Sort, S. E. Pratsinis, B. J. Nelson, M. S. Sakar, S. Pané, *ACS Appl. Mater. Interfaces* **2015**, *7*, 6803.

[49] D. Buenger, F. Topuz, J. Groll, *Prog. Polym. Sci.* **2012**, *37*, 1678.

[50] J. Li, D. J. Mooney, *Nat. Rev. Mater.* **2016**, *1*, 16071.

[51] K. Y. Lee, D. J. Mooney, *Chem. Rev.* **2001**, *101*, 1869.

[52] S. J. Jeon, A. W. Hauser, R. C. Hayward, *Acc. Chem. Res.* **2017**, *50*, 161.

[53] X. Le, W. Lu, J. Zhang, T. Chen, *Adv. Sci.* **2019**, *6*, 1801584.

[54] H. L. Lim, J. C. Chuang, T. Tran, A. Aung, G. Arya, S. Varghese, *Adv. Funct. Mater.* **2011**, *21*, 55.

[55] T. Tanaka, I. Nishio, S.-T. Sun, S. Ueno-Nishio, *Science* **1982**, *218*, 467.

[56] P. Xue, H. K. Bisoyi, Y. Chen, H. Zeng, J. Yang, X. Yang, P. Lv, X. Zhang, A. Priimagi, L. Wang, X. Xu, Q. Li, *Angew. Chem. Int. Ed.* **2021**, *60*, 3390.

[57] P. Chen, Q. Ruan, R. Nasseri, H. Zhang, X. Xi, H. Xia, G. Xu, Q. Xie, C. Yi, Z. M. Sun, H. Shahsavan, W. Zhang, *Adv. Sci.* **2022**, *9*, 2204730.

[58] Y. S. Kim, M. Liu, Y. Ishida, Y. Ebina, M. Osada, T. Sasaki, T. Hikima, M. Takata, T. Aida, *Nat. Mater.* **2015**, *14*, 1002.

[59] X. Yang, W. Shi, Z. Chen, M. Du, S. Xiao, S. Qu, C. Li, *Adv. Funct. Mater.* **2023**, 2214394.

[60] C. Yu, Z. Duan, P. Yuan, Y. Li, Y. Su, X. Zhang, Y. Pan, L. L. Dai, R. G. Nuzzo, Y. Huang, H. Jiang, J. A. Rogers, *Adv. Mater.* **2013**, *25*, 1541.

[61] C. Ma, X. Le, X. Tang, J. He, P. Xiao, J. Zheng, H. Xiao, W. Lu, J. Zhang, Y. Huang, T. Chen, *Adv. Funct. Mater.* **2016**, *26*, 8670.

[62] K. Iwaso, Y. Takashima, A. Harada, *Nat. Chem.* **2016**, *8*, 625.

[63] B. Xue, M. Qin, T. Wang, J. Wu, D. Luo, Q. Jiang, Y. Li, Y. Cao, W. Wang, *Adv. Funct. Mater.* **2016**, *26*, 9053.

[64] T. J. White, D. J. Broer, *Nat. Mater.* **2015**, *14*, 1087.

[65] D. Broer, G. P. Crawford, S. Zumer, *Cross-Linked Liquid Crystalline Systems: From Rigid Polymer Networks to Elastomers*, CRC Press/Taylor & Francis, Boca Raton, **2011**.

[66] S. W. Ula, N. A. Traugutt, R. H. Volpe, R. R. Patel, K. Yu, C. M. Yakacki, *Liq. Cryst. Rev.* **2018**, *6*, 78.

[67] Y. Guo, H. Shahsavan, M. Sitti, *Adv. Mater.* **2020**, *32*, 2002753.

[68] Y. Guo, H. Shahsavan, Z. S. Davidson, M. Sitti, *ACS Appl. Mater. Interfaces* **2019**, *11*, 36110.

[69] H. Aharoni, Y. Xia, X. Zhang, R. D. Kamien, S. Yang, *Proc. Natl. Acad. Sci. U. S. A.* **2018**, *115*, 7206.

[70] F. Serra, M. A. Gharbi, Y. Luo, I. B. Liu, N. D. Bade, R. D. Kamien, S. Yang, K. J. Stebe, *Adv. Opt. Mater.* **2015**, *3*, 1287.

[71] L. T. de Haan, C. Sánchez-Somolinos, C. M. W. Bastiaansen, A. P. H. J. Schenning, D. J. Broer, *Angew. Chem. Int. Ed.* **2012**, *51*, 12469.

[72] N. P. Pinchin, C. Lin, C. A. Kinane, N. Yamada, A. Pena-francesch, H. Shahsavan, *Soft Matter* **2022**, *18*, 8063.

[73] H. Shahsavan, A. Aghakhani, H. Zeng, Y. Guo, Z. S. Davidson, A. Priimagi, M. Sitti, *Proc. Natl. Acad. Sci. U. S. A.* **2020**, *117*, 5125.

[74] L. T. De Haan, V. Gimenez-Pinto, A. Konya, T. S. Nguyen, J. M. N. Verjans, C. Sánchez-Somolinos, J. V. Selinger, R. L. B. Selinger, D. J. Broer, A. P. H. J. Schenning, *Adv. Funct.*

Mater. **2014**, *24*, 1251.

[75] D. Liu, C. W. M. Bastiaansen, J. M. J. Den Toonder, D. J. Broer, *Macromolecules* **2012**, *45*, 8005.

[76] T. H. Ware, M. E. McConney, J. J. Wie, V. P. Tondiglia, T. J. White, *Science.* **2015**, *347*, 982.

[77] O. M. Wani, R. Verpaalen, H. Zeng, A. Priimagi, A. P. H. J. Schenning, *Adv. Mater.* **2019**, *31*, 1805985.

[78] H. Zeng, O. M. Wani, P. Wasylczyk, R. Kaczmarek, A. Priimagi, *Adv. Mater.* **2017**, *29*, 1701814.

[79] O. M. Wani, H. Zeng, P. Wasylczyk, A. Priimagi, *Adv. Opt. Mater.* **2018**, *6*, 1700949.

[80] T. Zhao, Y. Zhang, Y. Fan, J. Wang, H. Jiang, J. Lv, *J. Mater. Chem. C* **2022**, *10*, 3796.

[81] L. Yu, H. Shahsavan, G. Rivers, C. Zhang, P. Si, B. Zhao, *Adv. Funct. Mater.* **2018**, *28*, 1802809.

[82] M. Zhang, H. Shahsavan, Y. Guo, A. Pena-Francesch, Y. Zhang, M. Sitti, *Adv. Mater.* **2021**, *33*, 2008605.

[83] C. M. Yakacki, M. Saed, D. P. Nair, T. Gong, S. M. Reed, C. N. Bowman, *RSC Adv.* **2015**, *5*, 18997.

[84] H. Finkelmann, *Angew. Chem. Int. Ed.* **1987**, *26*, 816.

[85] L. B. Braun, T. G. Linder, T. Hessberger, R. Zentel, *Polymers* **2016**, *8*, 435.

[86] A. Komp, J. Rühe, H. Finkelmann, *Macromol. Rapid Commun.* **2005**, *26*, 813.

[87] Y. Hong, A. Buguin, J. M. Taulemesse, K. Kaneko, S. Méry, A. Bergeret, P. Keller, *J. Am. Chem. Soc.* **2009**, *131*, 15000.

[88] S. Schuhladen, F. Preller, R. Rix, S. Petsch, R. Zentel, H. Zappe, *Adv. Mater.* **2014**, *26*, 7247.

[89] Y. Yao, J. T. Waters, A. V. Shneidman, J. Cui, X. Wang, N. K. Mandsberg, S. Li, A. C. Balazs, J. Aizenberg, *Proc. Natl. Acad. Sci. U. S. A.* **2018**, *115*, 12950.

[90] M. Tabrizi, T. H. Ware, M. R. Shankar, *ACS Appl. Mater. Interfaces* **2019**, *11*, 28236.

[91] D. Liu, C. W. M. Bastiaansen, J. M. J. Den Toonder, D. J. Broer, *Angew. Chem. Int. Ed.* **2012**,

51, 892.

[92] H. Jiang, C. Li, X. Huang, *Nanoscale* **2013**, *5*, 5225.

[93] L. Qin, X. Liu, Y. Yu, *Adv. Opt. Mater.* **2021**, *9*, 2001743.

[94] S. Ustunel, M. E. Prévôt, R. J. Clements, E. Hegmann, *Liq. Cryst. Today* **2020**, *29*, 40.

[95] D. Martella, C. Parmeggiani, *Chem. Eur. J.* **2018**, *24*, 12206.

[96] M. Fallah-Darrehchi, P. Zahedi, P. Harirchi, M. Abdouss, *ACS Appl. Polym. Mater.* **2023**, *5*, 1076.

[97] W. Xie, R. Ouyang, H. Wang, N. Li, C. Zhou, *Liq. Cryst.* **2020**, *47*, 449.

[98] R. K. Shaha, D. R. Merkel, M. P. Anderson, E. J. Devereaux, R. R. Patel, A. H. Torbati, N. Willett, C. M. Yakacki, C. P. Frick, *J. Mech. Behav. Biomed. Mater.* **2020**, *107*, 103757.

[99] S. Dieterich, F. Stemmler, N. Preisig, F. Giesselmann, *Adv. Mater.* **2021**, *33*, 2007340.

[100] K. Steck, S. Dieterich, C. Stubenrauch, F. Giesselmann, *J. Mater. Chem. C* **2020**, *8*, 5335.

[101] R. S. Kularatne, H. Kim, M. Ammanamanchi, H. N. Hayenga, T. H. Ware, *Chem. Mater.* **2016**, *28*, 8489.

[102] J. M. Boothby, J. Samuel, T. H. Ware, *Soft Matter* **2019**, *15*, 4508.

[103] C. F. Dietrich, P. J. Collings, T. Sottmann, P. Rudquist, F. Giesselmann, *Proc. Natl. Acad. Sci. U. S. A.* **2020**, *117*, 27238.

[104] K.-Y. Law, *J. Phys. Chem. Lett.* **2014**, *5*, 686.

[105] S. Herrera-Posada, C. Mora-Navarro, P. Ortiz-Bermudez, M. Torres-Lugo, K. M. McElhinny, P. G. Evans, B. O. Calcagno, A. Acevedo, *Mater. Sci. Eng. C* **2016**, *65*, 369.

[106] D. Liu, L. Liu, P. R. Onck, D. J. Broer, *Proc. Natl. Acad. Sci. U. S. A.* **2015**, *112*, 3880.

[107] D. Liu, *Adv. Opt. Mater.* **2019**, *7*, 1900255.

[108] N. T. Correia, J. J. Moura Ramos, M. H. C. V. Adão, B. J. V. Saramago, *Mol. Cryst. Liq. Cryst.* **1997**, *300*, 45.

[109] Celanese Corporation, *Vectra LCP Design Guide*, **2013**.

[110] R. Rihani, N. Tasnim, M. Javed, J. O. Usoro, T. M. D'Souza, T. H. Ware, J. J. Pancrazio, *Neuromodulation* **2022**, *25*, 1259.

[111] J. Jeong, S. W. Lee, K. S. Min, S. Shin, S. B. Jun, S. J. Kim, *Sensors Mater.* **2012**, *24*, 189.

[112] C. Hassler, T. Boretius, T. Stieglitz, *J. Polym. Sci. Part B Polym. Phys.* **2011**, *49*, 255.

[113] G. Flodberg, L. Höjvall, M. S. Hedenqvist, E. R. Sadiku, U. W. Gedde, *Int. J. Polym. Mater. Polym. Biomater.* **2001**, *49*, 157.

[114] A. Sánchez-Ferrer, T. Fischl, M. Stubenrauch, H. Wurmus, M. Hoffmann, H. Finkelmann, *Macromol. Chem. Phys.* **2009**, *210*, 1671.

[115] Y. Yu, M. Nakano, T. Ikeda, *Nature* **2003**, *425*, 145.

[116] T. Ikeda, M. Nakano, Y. Yu, O. Tsutsumi, A. Kanazawa, *Adv. Mater.* **2003**, *15*, 201.

[117] A. H. Gelebart, G. Vantomme, E. W. Meijer, D. J. Broer, *Adv. Mater.* **2017**, *29*, 1606712.

[118] H. Wermter, H. Finkelmann, *e-Polymers* **2001**, *13*, 1.

[119] M. O. Saed, C. P. Ambulo, H. Kim, R. De, V. Raval, K. Searles, D. A. Siddiqui, J. M. O. Cue, M. C. Stefan, M. R. Shankar, T. H. Ware, *Adv. Funct. Mater.* **2019**, *29*, 1806412.

[120] R. Yang, Y. Zhao, *Angew. Chem. Int. Ed.* **2017**, *56*, 14202.

[121] M. J. Ford, M. Palaniswamy, C. P. Ambulo, T. H. Ware, C. Majidi, *Soft Matter* **2020**, *16*, 5878.

[122] Z. C. Jiang, Y. Y. Xiao, J. B. Hou, X. S. Chen, N. Yang, H. Zeng, Y. Zhao, *Angew. Chem. Int. Ed.* **2022**, *61*, e202211959.

[123] S. Palagi, A. G. Mark, S. Y. Reigh, K. Melde, T. Qiu, H. Zeng, C. Parmeggiani, D. Martella, A. Sanchez-Castillo, N. Kapernaum, F. Giesselmann, D. S. Wiersma, E. Lauga, P. Fischer, *Nat. Mater.* **2016**, *15*, 647.

[124] O. M. Wani, H. Zeng, A. Priimagi, *Nat. Commun.* **2017**, *8*, 15546.

[125] H. Zeng, O. M. Wani, P. Wasylczyk, A. Priimagi, *Macromol. Rapid Commun.* **2018**, *39*, 1700224.

[126] D. Martella, S. Nocentini, D. Nuzhdin, C. Parmeggiani, D. S. Wiersma, *Adv. Mater.* **2017**, *29*,

1705047.

[127] Y. Wang, Q. Guan, D. Lei, R. Esmaeely Neisiany, Y. Guo, S. Gu, Z. You, *ACS Nano* **2022**, *16*, 19393.

[128] Z. C. Jiang, Y. Y. Xiao, R. D. Cheng, J. B. Hou, Y. Zhao, *Chem. Mater.* **2021**, *33*, 6541.

[129] C. Ahn, K. Li, S. Cai, *ACS Appl. Mater. Interfaces* **2018**, *10*, 25689.

[130] Z. Hu, Y. Li, J. an Lv, *Nat. Commun.* **2021**, *12*, 3211.

[131] Q. He, Z. Wang, Y. Wang, Z. Wang, C. Li, R. Annapooranan, J. Zeng, R. Chen, S. Cai, *Sci. Robot.* **2021**, *6*, eabi9704.

[132] H. Tian, Z. Wang, Y. Chen, J. Shao, T. Gao, S. Cai, *ACS Appl. Mater. Interfaces* **2018**, *10*, 8307.

[133] M. Camacho-Lopez, H. Finkelmann, P. Palffy-Muhoray, M. Shelley, *Nat. Mater.* **2004**, *3*, 307.

[134] X. Yang, Y. Chen, X. Zhang, P. Xue, P. Lv, Y. Yang, L. Wang, W. Feng, *Nano Today* **2022**, *43*, 101419.

[135] Z. Deng, H. Zhang, A. Priimagi, H. Zeng, *Adv. Mater.* **2023**, 2209683.

[136] H. M. D. Bandara, S. C. Burdette, *Chem. Soc. Rev.* **2012**, *41*, 1809.

[137] A. A. Beharry, O. Sadovski, G. A. Woolley, *J. Am. Chem. Soc.* **2011**, *133*, 19684.

[138] C. Knie, M. Utecht, F. Zhao, H. Kulla, S. Kovalenko, A. M. Brouwer, P. Saalfrank, S. Hecht, D. Bléger, *Chem. Eur. J.* **2014**, *20*, 16492.

[139] D. B. Konrad, G. Savasci, L. Allmendinger, D. Trauner, C. Ochsenfeld, A. M. Ali, *J. Am. Chem. Soc.* **2020**, *142*, 6538.

[140] K. Kuntze, J. Viljakka, E. Titov, Z. Ahmed, E. Kalenius, P. Saalfrank, A. Priimagi, *Photochem. Photobiol. Sci.* **2022**, *21*, 159.

[141] S. Iamsaard, E. Anger, S. J. Aßhoff, A. Depauw, S. P. Fletcher, N. Katsonis, *Angew. Chem. Int. Ed.* **2016**, *55*, 9908.

[142] M. del Pozo, L. Liu, M. Pilz da Cunha, D. J. Broer, A. P. H. J. Schenning, *Adv. Funct. Mater.*

2020, *30*, 2005560.

[143] R. C. P. Verpaalen, M. Pilz da Cunha, T. A. P. Engels, M. G. Debije, A. P. H. J. Schenning, *Angew. Chem. Int. Ed.* **2020**, *59*, 4532.

[144] L. Liu, M. del Pozo, F. Mohseninejad, M. G. Debije, D. J. Broer, A. P. H. J. Schenning, *Adv. Opt. Mater.* **2020**, *8*, 2000732.

[145] M. Pilz Da Cunha, E. A. J. Van Thoor, M. G. Debije, D. J. Broer, A. P. H. J. Schenning, *J. Mater. Chem. C* **2019**, *7*, 13502.

[146] Z. Hu, W. Fang, Q. Li, X. Q. Feng, J. an Lv, *Nat. Commun.* **2020**, *11*, 5780.

[147] S. Ma, X. Li, S. Huang, J. Hu, H. Yu, *Angew. Chem. Int. Ed.* **2019**, *58*, 2655.

[148] C. L. Van Oosten, C. W. M. Bastiaansen, D. J. Broer, *Nat. Mater.* **2009**, *8*, 677.

[149] A. H. Gelebart, M. Mc Bride, A. P. H. J. Schenning, C. N. Bowman, D. J. Broer, *Adv. Funct. Mater.* **2016**, *26*, 5322.

[150] B. Xu, C. Zhu, L. Qin, J. Wei, Y. Yu, *Small* **2019**, *15*, 1901847.

[151] Q. Liu, G. Yu, C. Zhu, B. Peng, R. Li, T. Yi, Y. Yu, *Small Methods* **2021**, *5*, 2100969.

[152] Y. Lu, L. Qin, Q. Liu, Z. Li, W. Zhang, C. Zhu, Y. Yu, *NPG Asia Mater.* **2022**, *14*, 73.

[153] E. M. Purcell, *Am. J. Phys.* **1977**, *45*, 3.

[154] J. Zhang, Y. Guo, W. Hu, M. Sitti, *Adv. Mater.* **2021**, *33*, 2100336.

[155] J. Zhang, Y. Guo, W. Hu, R. H. Soon, Z. S. Davidson, M. Sitti, *Adv. Mater.* **2021**, *33*, 2006191.

[156] J. W. M. Bush, D. L. Hu, *Annu. Rev. Fluid Mech.* **2006**, *38*, 339.

[157] E. Lauga, A. M. J. Davis, *J. Fluid Mech.* **2012**, *705*, 120.

[158] A. Pena-Francesch, J. Giltinan, M. Sitti, *Nat. Commun.* **2019**, *10*, 3188.

[159] B. Kwak, S. Choi, J. Maeng, J. Bae, *Sci. Rep.* **2021**, *11*, 17469.

[160] C. H. Meredith, A. C. Castonguay, Y. J. Chiu, A. M. Brooks, P. G. Moerman, P. Torab, P. K. Wong, A. Sen, D. Velegol, L. D. Zarzar, *Matter* **2022**, *5*, 616.

[161] Y. Ikezoe, G. Washino, T. Uemura, S. Kitagawa, H. Matsui, *Nat. Mater.* **2012**, *11*, 1081.

[162] N. Bassik, B. T. Abebe, D. H. Gracias, *Langmuir* **2008**, *24*, 12158.

[163] M. L. Timm, S. J. Kang, J. P. Rothstein, H. Masoud, *Bioinspiration and Biomimetics* **2021**, *16*, 066014.

[164] C. Ahn, X. Liang, S. Cai, *Adv. Mater. Technol.* **2019**, *4*, 1900185.

[165] M. Rogó, K. Dradrach, C. Xuan, P. Wasylczyk, *Macromol. Rapid Commun.* **2019**, *40*, 1900279.

[166] H. Zeng, P. Wasylczyk, D. S. Wiersma, A. Priimagi, *Adv. Mater.* **2018**, *30*, 1703554.

[167] M. Pilz da Cunha, S. Ambergen, M. G. Debije, E. F. G. A. Homburg, J. M. J. den Toonder, A. P. H. J. Schenning, *Adv. Sci.* **2020**, *7*, 1902842.

[168] L. Dong, Y. Zhao, *Mater. Chem. Front.* **2018**, *2*, 1932.

[169] H. Shahsavan, S. M. Salili, A. Jákli, B. Zhao, *Adv. Mater.* **2015**, *27*, 6828.

[170] I. Colomer, A. E. R. Chamberlain, M. B. Haughey, T. J. Donohoe, *Nat. Rev. Chem.* **2017**, *1*, 88.

[171] A. Pena-Francesch, S. Florez, H. Jung, A. Sebastian, I. Albert, W. Curtis, M. C. Demirel, *Adv. Funct. Mater.* **2014**, *24*, 7401.

[172] A. Pena-Francesch, N. E. Domeradzka, H. Jung, B. Barbu, M. Vural, Y. Kikuchi, B. D. Allen, M. C. Demirel, *APL Mater.* **2018**, *6*, 10701.

[173] A. Pena-Francesch, M. C. Demirel, *Front. Chem.* **2019**, *7*, 69.

[174] A. Pena-Francesch, H. Jung, M. C. Demirel, M. Sitti, *Nat. Mater.* **2020**, *19*, 1230.

[175] A. Lebar, G. Cordoyiannis, Z. Kutnjak, B. Zalar, in *Liquid Crystal Elastomers: Materials and Applications*, Springer, Heidelberg **2010**, 147–185.

[176] K. Kumar, C. Knie, D. Bléger, M. A. Peletier, H. Friedrich, S. Hecht, D. J. Broer, M. G. Debije, A. P. H. J. Schenning, *Nat. Commun.* **2016**, *7*, 11975.

[177] T. Ohzono, H. Minamikawa, E. Koyama, Y. Norikane, *Adv. Mater. Interfaces.* **2021**, *8*, 2100672

[178] Y. L. Tae, A Multi-Function, Microfluidic Module for Mutation Detection, **2009**.

[179] K. V. Sharp, R. J. Adrian, J. G. Santiago, J. I. Molho, in *MEMS: Introduction and Fundamentals*, CRC Press, Boca Raton, **2005**.

[180] P. G. De Gennes, J. Prost, *The Physics of Liquid Crystals*, Oxford University Press, Oxford, **1993**.

[181] P. P. Marín San Román, R. P. Sijbesma, *Adv. Mater. Interfaces* **2022**, *9*, 2200341.

[182] J. A. M. Lugger, P. P. Marín San Román, C. C. E. Kroonen, R. P. Sijbesma, *ACS Appl. Mater. Interfaces* **2021**, *13*, 4385.

[183] C. S. Paik, H. Morawetz, *Macromolecules* **1972**, *5*, 171.

Appendix A

Iron Platinum Nanoparticles

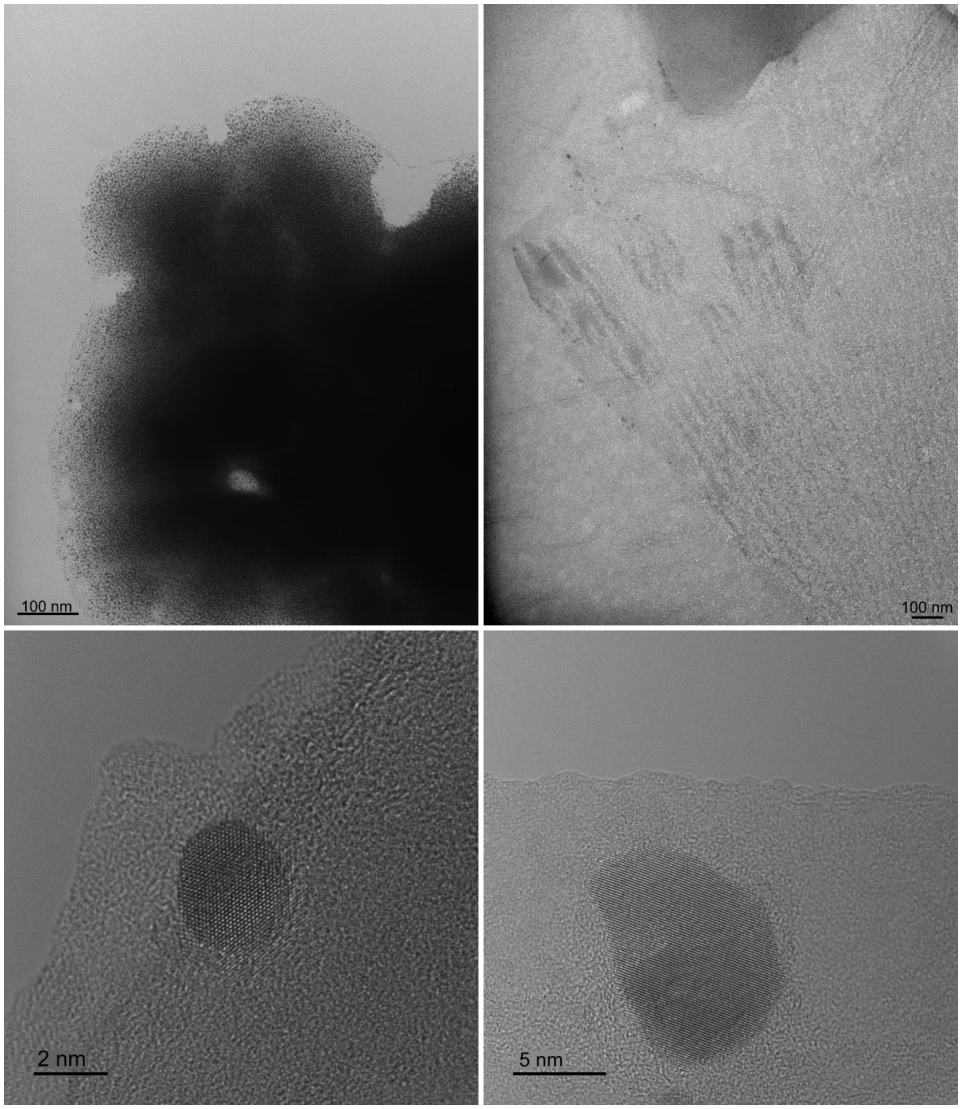


Figure A-1 TEM images of the ferromagnetic iron platinum nanoparticles